Quantum phases driven by strong correlations

Silke Paschen[1,2] and Qimiao Si[2]

[1]Institute of Solid State Physics, Vienna University of Technology, 1040 Vienna, Austria

[2]Department of Physics and Astronomy, Rice University, Houston, TX 77005, USA

It has long been thought that strongly correlated systems are adiabatically connected to their noninteracting counterpart. Recent developments have highlighted the fallacy of this traditional notion in a variety of settings. Here we use a class of strongly correlated electron systems as a platform to illustrate the kind of quantum phases and fluctuations that are created by strong correlations. Examples are quantum critical states that violate the Fermi liquid paradigm, unconventional superconductivity that goes beyond the BCS framework, and topological semimetals induced by the Kondo interaction. We assess the prospect of designing other exotic phases of matter, by utilizing alternative degrees of freedom or alternative interactions, and point to the potential of these correlated states for quantum technology.

E-mails: paschen@ifp.tuwien.ac.at, qmsi@rice.edu

I. INTRODUCTION

This review is motivated by a number of recent developments in the field of strongly correlated electron systems that have created considerable excitement in the community, and may stimulate progress also in adjacent fields. One of the key open problems is the understanding of high-temperature superconductivity. The recent discovery of a change in the carrier density at the pseudogap critical point in a cuprate superconductor near optimal doping[1] suggests a compelling link to the selective $4f$ Mott transition in heavy fermion compounds across Kondo destruction quantum critical points (QCPs)[2–7], which may also feature a dome of high-temperature superconductivity[8]. Similar phenomena are observed in an organic superconductor[9] and, tentatively, in twisted bilayer graphene[10], further underpinning the need for a unified understanding. Common principles are also surfacing with respect to orbital physics. Being well established in transition metal oxides[11], orbitals are frequently

entwined with other degrees of freedom and may thus reveal their character only in the low-energy excitations. Examples are the iron-based superconductors[12], the hidden order phase in URu_2Si_2[13], or the sequential localization in an SU(4)-type heavy fermion system[14]. Finally, there is a surge of work on the interplay of strong correlations and topology. At focus so far have been quantum spin liquids and topological insulators and semimetals in transition metal compounds[15–17], Weyl-Kondo semimetals in heavy fermion systems[18,19], and renormalized Dirac fermions in twisted bilayer graphene[10]. It is expected that in the strong correlation regime, a wealth of entirely new phases—not adiabatically connected to those known in noninteracting systems—will be discovered, and push the frontiers of science much like the discovery of the fractional quantum Hall effect[20] did in 2-dimensional (2D) insulators.

So what is it that makes strongly correlated electron systems such a fertile ground for discovery? Electrons are considered as strongly correlated when their mutual Coulomb interaction is of the same order as their kinetic energy. This does not only make the problem challenging—as simple one-electron theories will fail—but rich. Tipping the balance between these two energies may change the system's ground state as well as the nature of its low-energy excitations. A particularly promising setting for emergent phenomena are continuous zero-temperature phase transitions. They generate quantum critical fluctuations which, in turn, may produce exotic excitations and novel phases. As suggested by these considerations, strongly correlated electron systems have been providing a rich setting for conceptual and theoretical advances. Examples include highly entangled phases of matter[21] and QCPs that go beyond the Landau framework[22–24].

In Fig. 1 we introduce different materials classes hosting strongly correlated electrons. Prominent representatives are the cuprate high-T_c superconductors[25], ruthenates and other transition metal oxides[11], heavy fermion systems[26], iron-based superconductors[12], organics[9], and low-dimensional materials[10]. The relevant electron orbitals in these systems are typically d or f orbitals which, unlike s or p orbitals, keep some degree of localization in the solid and thus lead to enhanced Coulomb interaction, and reduced band widths. In addition, at appropriate filling, they give rise to localized moments. In Sect. II we describe how these lead to the low-energy degrees of freedom which—together with the conduction electrons, phonons, and other excitations present also in weakly correlated cases—are the "building blocks" of correlated matter. The mutual interactions between them, together

with the symmetry defined by the hosting crystal structure, result in an overwhelming richness in physical properties. A key goal of the community is to trace these properties back to the various magnetic, superconducting, and topological phases (for representative phase diagrams, see Fig. S1), and transitions between them, to ultimately allow to create functionality via materials design. As we will discuss in Sect. III, a viable approach towards this goal is to apply non-thermal control parameters such as pressure or field to a given material to tune it across its various phases, and to follow the evolution of its properties. We will show that the extreme "softness" of heavy fermion compounds to external parameters makes them particularly suitable for such studies. The quantum phases and fluctuations that have been discovered by such investigations are discussed in Sect. IV. In Sect. V we describe new horizons in the field, addressing the potential of alternative tuning parameters, additional degrees of freedom and interactions beyond the canonical spin–conduction electron form, and the role of topology. Implications of insight gained from studying heavy fermion systems on other classes of correlated materials and, more generally, correlated states of matter are discussed in Sect. VI. We close with a summary and outlook in Sect. VII.

II.   BUILDING BLOCKS OF CORRELATED MATTER

In strongly correlated electron systems, the "onsite" Coulomb repulsion—between electrons associated with the same lattice site—is comparable or larger than the width of the noninteracting energy band. Thus, such atomic-level electron-electron interactions cannot be taken as a mere perturbation. Instead, they are more appropriately treated at the zeroth order, and a set of atomic levels ensues. These are energetically so far apart from each other that only the lowest ones can directly influence the thermodynamic or dynamical properties at low energies. The quantum numbers of these low-lying atomic levels, together with those of delocalized excitations such as itinerant electrons or acoustic phonons, specify the fundamental degrees of freedom—the building blocks—of the system (Fig. 1).

A familiar example is the Mott insulator in $3d$ transition metal systems. In the simplest case, where only one $3d$ orbital is important for any given lattice site, there is on average one electron per orbital (half-filled case), and the onsite Coulomb repulsion U is larger than the bare electron bandwidth. The lowest-energy atomic level, a doublet with the degeneracy given by the spin degree of freedom, is then occupied by a single electron; this corresponds

to a localized quantum spin $S = \frac{1}{2}$. Accessing the high-energy atomic levels amounts to creating or removing an electron from the singly-occupied doublet. Because this costs an energy on the order of $\frac{U}{2}$, these are high-energy electronic excitations (responsible for the Hubbard bands) and do not directly contribute to the low-energy properties. They do, however, mediate superexchange interactions between the localized moments.

Another example arises in the $4f$ electron-based heavy fermion systems. The strong onsite Coulomb repulsion of the $4f$ electrons, in combination with the large spin-orbit coupling and crystal electric field (CEF) effects, frequently lead to a Kramers doublet as the lowest-lying atomic level, again giving rise to localized moments of effective spin $S = \frac{1}{2}$. These moments interact with a separate band of *spd* electrons, in the form of an antiferromagnetic Kondo interaction, and with each other through a Ruderman-Kittel-Kasuya-Yosida (RKKY) spin-exchange interaction that is mediated by the conduction electron spin polarization[27].

The presence of these well-defined building blocks and their interactions have several implications. The Kondo and RKKY energy scales are small—much smaller than the bare conduction electron bandwidth (Box 1 in supplementary materials)—making the heavy fermion systems highly tunable and, in turn, a prototype model setting for studying quantum criticality. In addition, the clear understanding of the building blocks facilitates sharp theoretical analyses. Thus, we use heavy fermion systems as a prototype setting for our discussion of tuning and quantum criticality.

III. TUNING HEAVY FERMION SYSTEMS

There is a vast amount of correlated materials to be explored. This is due to the large number of d and f elements in the periodic table which are—at least in bulk materials—generally constituents of correlated materials, and the numerous crystal structures of binary, ternary, quaternary (...) compounds that may combine these elements with each other and with s and p elements. Indeed, it is important to sample this huge "phase space" of correlated materials at vastly different positions, to discover overarching principles and test for universality. However, an alternative approach to this "zoology" has proven particularly instructive: to (quasi-)continuously monitor the evolution of a given system's properties along a specific path in the phase space. As will be described in what follows such "tuning" studies have proven to be a successful strategy to advance the field.

One goal of tuning studies is to establish the different phases or ground states a given material system can adopt. A few examples of phase diagrams, displaying the phase transition temperatures of the system as function of a non-thermal tuning or control parameter, are shown in Fig. S1 of the supplementary materials. This provides an overview and allows to relate the observed physical properties to the different phases, or even to certain parts of a given phase (e.g., center or border of the phase). Typical tuning parameters are chemical substitutions within a family of isostructural compounds, doping as a special case thereof, or the application of external parameters such as pressure or magnetic field. Depending on the materials class, only modest or very large variations of these parameters are needed to appreciably change the properties of the system.

A materials class that is particularly responsive to such stimuli are heavy fermion compounds. This is attributed to the presence of (at least) the aforementioned two competing energy scales, the Kondo and the RKKY interaction[27]. As already considered by Doniach for the simplified situation of a one-dimensional Kondo lattice[28], tipping the balance between the two scales is expected to tune the system from an antiferromagnetic to a paramagnetic state. Indeed, numerous studies on heavy fermion metals have identified such transitions[29–34].

Vital for establishing systematics, and thus for laying the ground for a universal understanding, was the identification of a few simple, experimentally well-defined, and meaningful characteristics of the studied materials. Since early on[35] it is known that many heavy fermion metals show Fermi liquid properties at low temperatures. The typically measured quantities are the electrical resistivity, magnetic susceptibility, and specific heat. Their Fermi liquid forms[27] are $\rho = \rho_0 + AT^2$, $\chi = \chi_0$, and $c = \gamma T$. The correlation strength, quantified by the renormalized effective mass m^* of the charge carriers, enters in all three expressions, to first approximation as $A \sim (m^*)^2$, $\chi_0 \sim m^*$, and $\gamma \sim m^*$. As such, the experimental determination of A, χ_0, and γ allows to categorize heavy fermion metals according to their degree of correlation. Assembling data of numerous heavy fermion metals in γ vs χ_0 (Sommerfeld-Wilson) and A vs γ (Kadowaki-Woods) plots confirmed the theoretically expected universal ratios[36], in particularly neat form if corrections due to different ground state degeneracies[37] and effects of dimensionality, electron density, and anisotropy[38] are taken into account (Fig. 2a).

Further insight was gained with the discovery that the Fermi liquid parameters of even a single given material can be widely varied by the application of external tuning parameters.

As illustrated with two examples in Fig. 2b,c, in addition to ranges in tuning parameter where the effective mass is continuously or "adiabatically" varied, there are "neuralgic" points where the effective mass appears to diverge. Clearly, at such points, something extraordinary must be going on, and this is by now known to be the presence of a QCP. Quantum critical fluctuations emerging from a QCP lead to temperature dependencies distinct from Fermi liquid behavior, as will be further discussed in Sect. IV. The above-described divergence of the Fermi liquid parameters on approaching a QCP is a valuable diagnostic tool thereof.

IV.   QUANTUM PHASES AND FLUCTUATIONS

A QCP appears as the ground state of a quantum many-body system smoothly transforms from one state to another. Typical of the systems we consider in this article is a gradual suppression of an electronic ordered phase (Fig. 3a). On general grounds, entropy accumulates near a QCP. This follows from hyperscaling: The free energy density, with the dimension of energy/volume, is expected to have a singular component of the form $\frac{k_\mathrm{B}T}{\xi^d}$ multiplied by a universal scaling function of $\frac{|p-p_\mathrm{c}|}{\xi^{-1/\nu}}$ (here ξ is the correlation length, d the spacial dimension, ν the correlation length exponent and, for concreteness, we consider the tuning parameter δ to be linearly coupled to pressure p). It follows from this scaling form that the Grüneisen ratio as a function of p is maximized near p_c[39] and so is the entropy S (more precisely, the ratio S/T) for a sufficient low T, Fig. 3b[40].

The enhanced entropy makes the electron system particularly "soft", thereby promoting the nucleation of novel excitations and phases. For instance, strongly correlated metals display an unusual temperature dependence of the electrical resistivity at the QCP, reflecting the breakdown of the Landau quasiparticle concept and the ensuing formation of a non-Fermi liquid ("strange metal"). In addition, unconventional superconductivity often develops near a QCP. As such, quantum criticality rises to the level of a unifying theme for the description of the often exotic properties across a variety of strongly correlated materials[32,34,41,42].

In practice, quantum criticality often develops in bad metals and in the vicinity of antiferromagnetic order. A bad metal is specified by its resistivity at room temperature being large, reaching the Mott-Ioffe-Regel limit, which implicates the presence of strong electron correlations[43]. Such correlations cause a reduction in the coherent part of the electron spectral weight, as measured by angle resolved photoemission spectroscopy (ARPES)[44] and

6

optical conductivity[45,46]. Because a sufficiently large correlation strength suppresses the coherent electron part, it may lead to an electronic localization–delocalization transition. All these phenomena are exemplified by heavy fermion metals, which are canonical examples of bad metals and in which antiferromagnetic QCPs are especially prevalent[26,29–34]. We thus discuss these systems in what follows.

A. Quantum criticality

Consider a Kondo lattice (see Box 1 of supplementary materials), comprising a localized moment for each unit cell and a band of conduction electrons (Fig. 4a,b). When the RKKY interaction dominates over the Kondo coupling, the local moments develop static order and form an antiferromagnetic state (Fig. 4a). Deep in this state, it has been rigorously shown that the Kondo coupling is "exactly marginal" in the renormalization-group sense[47]; here, spin singlets are well established among the local moments, which are detrimental to the development of a Kondo singlet between the local moments and conduction electrons. The Fermi surface is then formed of the conduction electrons only—this is named a "small" Fermi surface (Fig. 4c).

In the opposite limit, when the Kondo coupling dominates over the RKKY interaction, the local moments form a spin singlet state with the conduction electrons (Fig. 4b). This is the standard paramagnetic heavy fermion state, characterized by a static Kondo-singlet amplitude. The ensuing Kondo entanglement of the local moments with the conduction electrons effectively turns the former into mobile carriers: A local moment and a conduction electron form a fermionic composite, which corresponds to a delocalized heavy electronic excitation. Its hybridization with the conduction electron band (Fig. 4f-h) produces the heavy quasiparticles. Thus, in this limit, the Fermi surface incorporates both the local moments and conduction electrons, and is "large" (Fig. 4d).

What is remarkable is that the transformation from the small to the large Fermi surface can occur sharply, precisely at a continuous zero-temperature phase transition from an antiferromagnetically ordered to a paramagnetic heavy fermion state. In $YbRh_2Si_2$, an antiferromagnet with a low Néel temperature ($T_N = 0.07$ K), application of a small magnetic field weakens the antiferromagnetic order and continuously suppresses it at the critical field B_c (Fig. 2b). Hall effect measurements[3,5] imply a sudden jump in the extrapolated

zero-temperature limit, precisely at the QCP (Fig. 4e), consistent with a sudden change from the small to the large Fermi surface. At nonzero temperatures, the Hall results as well as thermodynamic measurements[48] identify a temperature scale $T^*(B)$ in the temperature–magnetic field phase diagram which, anchored by the Fermi-surface-jumping QCP, characterizes the finite-temperature crossovers. Scanning tunneling microscopy (STM) experiments have provided spectroscopic evidence for the $T^*(B)$ scale[49], where a critical slowing down was evidenced from a linewidth analysis.

Another experimental signature of this drastic effect was revealed by quantum oscillation measurements. $CeRhIn_5$ is an antiferromagnetic metal with a Néel temperature $T_N = 3.8\,K$[50]. Applying pressure weakens the antiferromagnetic order and induces superconductivity[8,51]. In magnetic fields above the superconducting upper critical field H_{c2} these studies[8,51] reveal an antiferromagnetic QCP near the same pressure p_c where the de Haas–van Alphen (dHvA) frequencies jump and the cyclotron mass diverges[4]. From a comparison with *ab initio* electronic structure calculations for $LaRhIn_5$ and $CeRhIn_5$ (with the Ce-$4f$ electrons in the core) it was concluded that the Fermi surface transforms from small at $p < p_c$ to large at $p > p_c$[4].

These striking experimental observations were anticipated by theoretical studies[22–24]. Analyzing the Kondo lattice model identified an unusual type of QCP, where a small-to-large Fermi surface jump occurs at the antiferromagnetic-paramagnetic phase boundary[22]. The quantum criticality then captures not only the fluctuations from a suppression of the antiferromagnetic order parameter, but also those associated with a destruction of the static Kondo effect.

Kondo destruction quantum criticality has another salient feature, an ω/T scaling in the spin dynamics. The collapse of the static Kondo singlet makes the QCP to be described by an interacting fixed point, where the universal physics depends on only $k_B T$ and no other energy scales[22,23]. Calculations on Kondo lattice models based on an extended dynamical mean-field theory (EDMFT) have produced such ω/T behavior in the dynamical spin susceptibility at the Kondo destruction QCP[22,52,53]. This provides the understanding of inelastic neutron scattering experiments on quantum critical $CeCu_{5.9}Au_{0.1}$ (Fig. 5a). Its parent compound $CeCu_6$ is a paramagnetic heavy fermion metal, and a substitution of less than 2% of Cu by Au induces antiferromagnetic order. In $CeCu_{5.9}Au_{0.1}$, the dynamical spin susceptibility displays ω/T scaling with a fractional critical exponent (Fig. 5a). In β-$YbAlB_4$, B/T scaling

8

has been shown in thermodynamic quantities[54] (Fig. 5c), but dynamical scaling could not yet be tested.

An exciting recent development came from terahertz spectroscopy measurements of the optical conductivity of $YbRh_2Si_2$, which demonstrate ω/T scaling in the charge channel (Fig. 5d)[7]. This was understood as a consequence of probing a Kondo destruction QCP: Because the Kondo effect involves also the charge degree of freedom, its destruction should also lead to ω/T scaling in the charge sector.

The above features are to be contrasted with expectations for quantum criticality within the Landau framework, which is of spin-density-wave (SDW) type[55–57]. Going across an SDW QCP from the paramagnetic side, the Fermi surface evolves smoothly: it folds by the continuously onsetting SDW order parameter. As a result, across this QCP, both the Hall coefficient and the quantum oscillation frequencies vary smoothly. Moreover, the SDW QCP is described by a Gaussian fixed point, and a dangerously irrelevant variable generates an effective energy scale other than k_BT. In turn, ω/T scaling is violated.

Following the tradition of the paramagnon theory[58], the SDW-type QCP is discussed for purely itinerant electron systems. In heavy fermion compounds, local moments are part of the building blocks for the low-energy physics. It has been stressed that, for the Kondo destruction QCP to arise, it is essential to treat the dynamical competition between the RKKY and Kondo interactions. For instance, while the static Kondo singlet amplitude vanishes as the Kondo destruction QCP is approached from the paramagnetic side, the Kondo correlations at nonzero frequencies smoothly evolve across the QCP[53,59]. This effect is essential for the stability of the Kondo-destroyed phase, and also provides the understanding of a mass enhancement in that phase.

In view of this dynamical competition between the RKKY and Kondo interactions it follows that even in heavy fermion metals described by an SDW QCP at the lowest energies, the Kondo destruction crossover scale T^*, though nonzero, can still be considerably smaller than the bare Kondo temperature scale T_K^0.[60] In this case, there is an extended temperature range $(T^* < T < T_K^0)$ over which Kondo destruction quantum criticality should dominate the singular physics. For instance, in $CeCu_2Si_2$, the dynamical spin susceptibility follows the $\omega/T^{3/2}$ scaling form predicted for a three-dimensional SDW QCP (Fig. 5b)[61], corresponding to a $T^{3/2}$ relaxation rate. However, this rate becomes linear in T already at $1\,K$ and above, pointing to $T^* \sim 1\,K$ and a sizable temperature range, $T^* < T < T_K^0 \sim 20\,K$ where the

dynamics may be described by Kondo destruction physics; additional ways to ascertain this possibility are needed.

These developments establish antiferromagnetic heavy fermion metals to be a prototype setting for quantum criticality beyond the Landau framework. The fact that such a form of unconventional quantum criticality takes place at a transition between two conventional phases has motivated studies of beyond-Landau QCPs in the context of quantum magnets[62]. From the correlated electron perspective, Kondo destruction signifies an electronic localization–delocalization transition; indeed, it has been shown that the Kondo destruction QCP features criticality in both the spin and the charge (or single-particle) channels[22,52,53,63–65]. We will discuss the significance of this physics for systems beyond heavy fermion metals in Sec. VIA. More broadly, the Kondo destruction QCP is also captured by the evolution of entanglement entropy[53,66,67]; exploring entanglement properties, perhaps using emulating set-ups based on cold atoms or mesoscopic devices, will deepen our understanding of this novel type of quantum criticality and its associated strong correlation physics.

B.   Unconventional superconductivity and other emergent phases

As we have highlighted, quantum criticality provides a mechanism to soften the electronic system and nucleate novel phases. A widely recognized case in point is the development of unconventional superconductivity[68,69]. In $CePd_2Si_2$, a dome of superconductivity is observed around a pressure-induced QCP[68]. This QCP was discussed as being of SDW type and the superconducting pairing was associated with antiferromagnetic paramagnons[70]. This led to the important question whether a Kondo destruction QCP can also promote superconductivity. Theoretical calculations suggest that this is indeed the case[71,72].

There are by now about fifty heavy fermion superconductors. Many of them seem to be driven by antiferromagnetic quantum criticality, but whether that is indeed the case and, if so, what is the nature of the underlying QCP, remains to be clarified in most cases. In $CeRhIn_5$, where a Kondo destruction QCP was evidenced at a critical pressure from (above-H_{c2}) dHvA experiments[4], superconductivity indeed appeared near that pressure[8,51], suggesting that it is driven by the Kondo destruction QCP. The optimal T_c is about 2.3 K (in zero field)[8,51], which is among the highest transition temperatures for $4f$ electron-based

heavy fermion superconductors.

$CeCu_2Si_2$ is the heavy fermion metal in which unconventional superconductivity was first discovered[73], with $T_c = 0.6\,K$. The magnetic fluctuation spectrum changes noticeably upon entering the superconducting state[74], an effect that was also studied in other heavy fermion superconductors[75]; this gives rise to a large gain in the magnetic exchange energy, which is about 20 times the superconducting condensation energy[74,76], thereby providing evidence that the quantum critical magnetic fluctuations are a major driving force for the development of unconventional superconductivity. It also implies a loss of kinetic energy of close to 20 times the superconducting condensation energy, which is compatible with pairing in the spin-singlet channel. In that case, the development of superconducting pairing weakens the Kondo-singlet correlation and, thus, transfers the f-electron spectral weight from low energies to above the Kondo-destruction energy scale T^*[76]. The precise form of the spin-singlet pairing order parameter has been reanalysed in recent years. A multi-orbital $d + d$ pairing[77,78] provides a natural understanding of the gap-like features that have recently been observed by measurements of the specific heat and superfluid stiffness at the lowest temperatures[79–81]. This pairing state obeys the prohibition of any onsite pairing amplitude by the Coulomb repulsion. It features a spin resonance in the superconducting state[74], and the correlation effect is expected to reduce its sensitivity to non-magnetic disorder[82]. The conventional s-wave pairing, which has also been invoked to explain the observed gap[80], faces a large energetic penalty. Extended s-wave pairings have also been considered[83,84]. For the Fermi surface of $CeCu_2Si_2$, they are expected to be nodal, with any spin resonance being away from the intraband nesting wavevector observed experimentally[82]. Microscopically, the $d + d$ pairing order parameter, an irreducible representation of the crystalline point group, comprises intraband and interband d-wave pairing components. It is the non-commuting nature of the two components that produces a full gap on the Fermi surface, which is analogous to what happens in the ^3He superfluid B-phase[78].

For a long time, no superconductivity was found in $YbRh_2Si_2$. This changed when the specific heat and magnetization were measured at ultralow temperatures[85]. An analysis of the coupling between nuclear and electronic spins led to the picture that, below $2\,mK$, superconductivity coexists with hybrid nuclear–electron order, which reduces the primary electronic order and, consequently, enhances quantum critical fluctuations.

Other forms of emergent phases may also develop near a QCP. In $CeRhIn_5$ at ambi-

ent pressure, quantum oscillation and Hall effect measurements provided evidence for a Kondo destruction QCP near $B_0^* \approx 30\,\mathrm{T}$[86], which is considerably below the field for the zero-temperature magnetic to paramagnetic transition, $B_{c0} \approx 50\,\mathrm{T}$. Near B_0^*, transport measurements in samples fabricated by focused ion beam etching have indicated the development of nematic correlations[87]. Whether static nematic order exists and, if so, whether it is nucleated by Kondo destruction quantum criticality are interesting questions that deserve further investigations.

V.   NEW HORIZONS

Many of the extensive developments on heavy fermion quantum criticality, reviewed above, correspond to the prototypical setting[28], i.e. the physics of the competition between Kondo and RKKY interaction in a (spin 1/2) Kondo lattice. It is becoming increasingly clear that some of the most interesting phenomena, such as quantum criticality associated with electron localization and the formation of novel phases, are not limited to this canonical case but can be generalized to much broader contexts. Some of these developments will be highlighted in this section.

A.   Frustration and dimensionality

The localization–delocalization transition discussed earlier originates from the different types of correlations that are promoted by the Kondo and RKKY interactions. The singlet formation among the spins in the antiferromagnetic state leads to a destruction of the static Kondo effect. When the degree of frustration G[88] is large, spin singlets among the local moments develop even in a quantum paramagnet[15–17] and will be detrimental to the formation of the Kondo entanglement. This line of consideration lead to a global phase diagram[89–92], featuring both J_{K} (or $J_{\mathrm{K}}N_{\mathrm{F}}$, see Box 1 in supplementary materials) and the frustration parameter G as non-thermal tuning parameters (Fig. 3c). At large values of G, when the Kondo coupling is not too large, the static Kondo singlet amplitude vanishes, and a paramagnetic phase with small Fermi surface, P_{S}, is stabilized, possibly in the form of a metallic spin liquid. Concrete theoretical studies of the global phase diagram in frustrated Kondo lattice models have been carried out, using a large-N method in the case of the

Shastry-Sutherland lattice[93] and through a quantum Monte Carlo technique for a model on the honeycomb lattice[94].

To link such theoretical phase diagrams to experiments, one should be able to quantify the degree of frustration and, ideally, continuously vary it by some external tuning parameter. In insulating quantum magnets the frustration strength can be quantified by the ratio of the paramagnetic Weiss temperature and the ordering temperature or, in a more sophisticated way, by modelling magnetic structure data to extract exchange interactions[95,96]. In heavy fermion systems, however, the local moment exchange interaction is typically dominated by the long-ranged RKKY interaction, and thus the conduction electrons and anisotropies in their densities of states at the Fermi level may also play an important role in defining the degree of frustration.

Yet, so far, frustration in heavy fermion systems is discussed mostly in terms of the more intuitive concept of local moments situated on (partially) frustrated lattices[97–103]. Examples are $Pr_2Ir_2O_7$ with a pyrochlore lattice of Pr atoms[97,103], $CeRhSn$[100] and $CePdAl$[99,102] with Ce atoms located on distorted kagome planes, and $HoInCu_4$ with an fcc lattice of the Ho atoms[104] (though the Kondo interaction in this low-carrier density system is likely negligible). In $Pr_2Ir_2O_7$, non-Fermi liquid behavior is observed above certain cutoffs in temperature and field (possibly due to spin freezing)[97,105], and could be due to spin liquid behavior or quantum criticality from a nearby magnetic QCP. In CeRhSn, thermodynamic properties show non-Fermi liquid behavior only within the frustrated plane[100], and its suppression under uniaxial pressure applied within the plane, which lifts the frustration[106]. This provides evidence for frustration-induced non-Fermi liquid behavior. In CePdAl, a region of non-Fermi liquid behavior was found in a pressure–magnetic field phase diagram, and associated with the P_S phase[102] (Fig. 8b). Regions of non-Fermi liquid behavior are, however, also seen in heavy fermion metals without any obvious element of geometric frustration[107,108]. In $YbRh_2(Si_{1.95}Ge_{0.05})_2$, a P_S phase was shown to be nested between an AF_S phase and a P_L phase[108], thus directly confirming trajectory III in the theoretical phase diagram (Fig. 3c). Further work is needed to understand how this P_S phase relates to the ones hinted at in the above geometrically frustrated local moment systems with much weaker Kondo interaction. A recent STM study on $Pr_2Ir_2O_7$ provided evidence for a P_L to P_S transition through the tuning of minute disorder potential on the nanoscale[103].

A new platform for the exploration of this physics are heavy fermion thin films. In

insulating local moment systems, quantum fluctuations are not only boosted by (geometrical) frustration but also by reduced dimensionality (Fig. 3d). Thus, in the search for materials in which the G parameter can be (quasi-)continuously varied, also systems with tunable dimensionality should be considered[6]. High-quality thin films grown by molecular beam epitaxy[7,109,110] appear as promising way forward. Superlattices of heavy fermion metals with normal metals ($CeIn_3/LaIn_3$ and $CeRhIn_5/YbRhIn_5$) indeed showed the emergence of non-Fermi liquid signatures with decreasing superlattice period[109,110]. Whether this represented the appearance of the P_S phase (along trajectory III in Fig. 3c), or quantum criticality from the suppression of antiferromagnetic order (along trajectory I in Fig. 3c) is an interesting question for future studies, including ideally also superlattices with passive (non-metallic) spacer compounds. In the opposite direction, one can reduce G by going to the three-dimensional limit. The cubic compound $Ce_3Pd_{20}Si_6$ fits this prescription. Magnetotransport and thermodynamic measurements have firmly established that the Kondo destruction appears within the ordered part of the phase diagram (Fig. 6a-c and Fig. 8a)[6].

B. Entwined degrees of freedom and hybrid interactions

We have so far considered the case of localized spins coupled to each other and to conduction electrons by spin-exchange interactions. The rich settings of condensed matter systems, however, allow us to utilize, or even design, alternative degrees of freedom. In heavy fermion systems, physics beyond the spin-only case comes in naturally: For the $4f$ ($5f$) electrons of the rare earth (actinide) elements, the intraatomic spin-orbit coupling is large, and thus having effective moments of total angular momentum $J > 1/2$, that encompass both spins (dipoles) and higher multipolar moments, is the generic case. Crystal electric fields split these spin-orbit coupled states, but even the ground state will, in general, not be a spin-only Kramers doublet.

An example is the cubic heavy fermion compound $Ce_3Pd_{20}Si_6$. Its $Ce4f^1$ crystal-field-split ground state is a Γ_8 quartet, which has multipolar character. Surprisingly simple low-energy behavior was observed[14]: Across two QCPs, one at the border of antiferromagnetic (AFM), the other at the border of antiferroquadrupolar (AFQ) order (Fig. 6a), two distinct electron localization transitions take place, driven by a single degree of freedom at a time (Fig. 6b,c). They were understood as a sequential destruction of an SU(4) spin-orbital-coupled Kondo

effect[14].

Also in other classes of strongly correlated electron systems there is ample evidence for entwined degrees of freedom. In the manganites[11] and fullerides[111], it is also spin and orbital degrees of freedom that interplay, and in the iron pnictides and chalcogenides, more than one $3d$ orbital is important for the physics near the Fermi energy[12]. In the cuprates, charge order emerges and interplays with the spin degrees of freedom[1,112], and even in magic-angle bilayer graphene, the physics likely depends on both the spin and valley degrees of freedom[10]. To advance the understanding of the rich physical phenomena present in all these materials, it is important to decipher the roles the different degrees of freedom play in determining the stable phases (Fig. S1 in supplementary materials) and excitations associated with them, as well as with (quantum) phase transitions between them.

Strong electron interactions can also be modified by other interactions. In fact, the competition between the different energy scales associated with the various degrees of freedom—that also leads to the rich phase diagrams (Fig. S1 in supplementary materials)—makes these systems generally highly responsive to all kinds of stimuli. Particularly interesting are situations where alternative interactions boost strong-correlation effects, thereby enhancing functionality.

One example is "phonon boosting". The interplay of the electron-electron Coulomb interaction and phonon-mediated electron interaction effects is captured by the Anderson-Holstein model[113], which has been much explored in the context of single molecular transistors[114,115]. In Kondo systems, increasing the coupling of the conduction electrons with local optical phonons was shown to enhance the Kondo temperature by orders of magnitude, up to a point beyond which the charge Kondo effect is stabilized[116]. This (former) mechanism was suggested to explain a high-temperature Kondo effect in a Ce-based thermoelectric "rattler" compound[117]. Its thermopower at room temperature was shown to be strongly enhanced over values found in a $4f$ moment-free reference compound (Fig. 6e) though the bare Kondo temperature of the system at low temperatures, where the rattling mode is not activated, was only $1\,\mathrm{K}$. This effect almost doubled the thermoelectric figure of merit[117]. The strong response to phonons in this type-I clathrate compound is due to its special crystal structure, with an atom trapped in an oversized cage. Whereas most heavy fermion compounds lack such special structure elements and are much less sensitive to phonons, other strongly correlated electron systems, in particular with polar bonds and/or

reduced dimensionality, do show phonon- (as well as photon-)boosting effects; these will be discussed in Sect. VI.

C. Correlation-driven topology

With the advent of "topology" in electronic materials[21,118–123] also the question of how strong correlations and topology may interplay is attracting much interest. In light of recent developments, we here focus on Weyl semimetals[121–123] (Box 2 in supplementary materials).

Theoretical predictions for noninteracting electron systems are becoming ever more efficient in guiding the search for new candidate materials. In principle, topological invariants— key quantities in defining the topological nature of the electrons' wavefunctions—can be directly calculated from electronic band structure. Because this is a laborious process, other, higher throughput methods were also developed. These classify materials by certain indicators for topology, most notably symmetry eigenvalues[124–128].

Despite—or even because—these approaches have by now identified enormous numbers of candidate materials, clear-cut experimental confirmations remain a formidable task. ARPES is playing a central role in it (see panels a-d in Box 2 in supplementary materials), even though the interpretation is not always easy. On one hand, to disentangle surface from bulk and topological from topologically trivial states, comparison with *ab initio* calculations is needed, which are challenging for real surfaces even in the noninteracting case. On the other hand, the rather intense incident light may "dope" the surface and thus modify the bandstructure[129]. Complementary experimental techniques, including (magneto)transport, optical spectroscopy, and quantum oscillation experiments, are thus equally important, and have indeed provided independent evidence[123,130–133].

To address the effect of correlations, theoretical treatments can either (i) study how electron correlations modify (known) noninteracting topological states, or (ii) explore how nontrivial topology can be introduced into (known) strongly correlated electronic states. A recent example in the spirit of approach (i) is an optical spectroscopy study of the nodal-line semimetal ZrSiSe[134], where a comparison with density functional theory (DFT) revealed a reduction of the Fermi velocity with respect to the noninteracting one derived by DFT by almost 30%, an effect that was attributed to interactions (Fig. 2d). Similar effects are seen also in several other topological semimetals (Fig. 2e); and also for graphene, a quantum

Monte Carlo study showed short- and long-range Coulomb interaction effects to reduce the Fermi velocity by about 40% near the strong-coupling fixed point[135].

As for Schrödinger particles, where even Fermi liquids with extreme renormalizations (by orders of magnitude, see Fig. 2a) may—but do not have to be (Fig. 2b,c)—adiabatically connected to the noninteracting state, one could conceive such a situation also for Dirac particles. Thus, approach (ii) may well discover phenomena that have no analogues in the noninteracting world, a particularly exciting prospect.

A promising setting to find such entirely new electronic phases are systems where strong electron correlations and large spin–orbit interaction coexist, as is the case in heavy fermion compounds. To single out the effect of the spin–orbit interaction, a strategy to selectively tune its strength should be identified. This attempt was made in a chemical substitution study of the Kondo insulator $Ce_3Bi_4Pt_3$ where the $5d$ element Pt was successively replaced by the $4d$ element Pd[18]. As this substitution is isostructural, isoelectronic, and essentially isosize, the large mass difference between Pt and Pd and the associated difference in atomic spin–orbit coupling strength was suggested to play the dominant role in the tuning[18]. A transformation from an insulator to a semimetal was observed with increasing Pd content, with the end compound $Ce_3Bi_4Pd_3$ showing striking signatures of nontrivial topology: The low-temperature electronic specific heat coefficient $\Delta C/T$ is linear in T^2 (Fig. 7a), pointing to a linear electronic dispersion in momentum space, as expected for Dirac or Weyl fermions. The velocity of the corresponding fermions calculated from the slope Γ is less than $1000\,\mathrm{m/s}$, which is three orders of magnitude lower than a typical Fermi velocity of simple metals. Because this unusual specific heat contribution appeared only below the Kondo temperature—which is again one thousandth of a typical Fermi temperature—it was argued to be Kondo-driven[18].

Indeed, a theoretical study of the periodic Anderson model on a noncentrosymmetric lattice discovered a Kondo-driven topological semimetal phase, dubbed Weyl-Kondo semimetal[19], with extremely flat linear dispersion around Weyl nodes pinned to the Fermi energy (Fig. 7b,c), in agreement with the above experiments[18]. The Kondo effect cooperates with the nonsymmorphic space group of the underlying lattice, not only to generate the strongly renormalized Weyl nodes but also to place them at the Fermi energy[136]. Weyl and anti-Weyl nodes are sources and sinks of Berry curvature (Fig. 7d). Recent experiments have directly evidenced them via spontaneous (zero magnetic field) Hall effect measurements[137],

and even seen them annihilate in large magnetic fields[138]. The giant magnitude of the spontaneous Hall effect, as well as its electric field and frequency dependence were understood as the Weyl nodes being part of the Kondo resonance, situated in immediate proximity to the Fermi energy[137]. The calculations[19] also predicted surface states that feature strongly renormalized Fermi arcs, which still await experimental confirmation.

Weyl physics is being explored also in other Ce- and Yb-based intermetallic compounds[139–141], creating the exciting opportunity to discover signatures of strong correlation-driven electronic topology also there. Together with theoretical efforts[136,142–150] this may help to establish the new field of strongly correlated electronic topology.

VI. BROADER IMPLICATIONS

We have highlighted how the heavy fermion systems provide a setting to search for and explore quantum criticality and novel quantum phases. Ultimately, the field of strongly correlated systems aims to develop the organizing principles that may operate across the materials platforms. With that consideration in mind, we discuss how the insights gained from the heavy fermion field impact on other classes of strongly correlated systems and beyond.

A. Quantum criticality and electronic localization–delocalization

In heavy fermion quantum criticality, the physics of Kondo destruction plays an essential role. From the critical phenomenon perspective, the Kondo destruction QCP involves critical physics that is beyond the Landau framework of order parameter fluctuations. The destruction of the static Kondo effect gives rise to critical modes that are in addition to the slow fluctuations of the antiferromagnetic order parameter. From the correlated electron perspective, this type of QCP epitomizes metallic quantum criticality in which the suppression of electronic orders entwines with an electronic localization–delocalization transition[2–7]. Such a transition of electrons in a metallic background, and its accompanying jump of Fermi surface, have also been emphasized in the context of hole-doped high T_c cuprates[1,112].

This analogy extends to the domain of theoretical analyses. In heavy fermion systems, the destruction of the static Kondo effect and the associated jump of the Fermi surface have

been extensively analyzed using the EDMFT approach to the Kondo lattice model[22,52,53]. A similar method has recently been adopted to describe the localization–delocalization transition in the single-band Hubbard model in the context of the high T_c cuprates[151,152].

The global phase diagram of heavy fermion systems delineates whether a jump of Fermi surface is concurrent with—or detached from—the suppression of antiferromagnetic or other electronic orders. Also in the case of high T_c cuprates, the relationship between a sudden reconstruction of the Fermi surface and the development of electronic orders at zero temperature is a central issue.

Additionally, the localization–delocalization transition comes into play near the Mott transition in Mott-Hubbard systems, as has been considered theoretically[153,154]. Organic charge-transfer salts have provided a versatile materials setting to study this issue. For example, measurements of the Hall coefficient in a doped organic superconductor, κ-ET$_4$Hg$_{2.89}$Br$_8$, have hinted at a drastic Fermi surface transformation[9]. In intermetallic systems, there has been considerable recent development on materials with a potential spin-liquid ground state. Pressurizing such compounds presents a promising new setting to realize a Mott transition and elucidate the accompanying evolution of the Fermi surface. Progress along this direction has recently been reported in a high-pressure study of NaYbSe$_2$ (Fig. 8e)[155].

The Kondo destruction QCP, with the localization–delocalization transition of the f electrons in a metallic background[22,23,156], represents the earliest example of orbital-selective Mott transitions. In d electron systems, this transition was first discussed in the context of the ruthenates[157]. Unlike in the heavy fermion case, the analysis was done in the band basis; different bands, by definition, do not hybridize with each other. In reality, the Coulomb interactions are expressed in the orbital basis, and crystalline symmetry generically allows for inter-orbital kinetic coupling. In that sense, the orbital-selective Mott transition in d electron systems shares one important aspect with what happens in the heavy fermion compounds: The realization of the orbital-selective Mott phase requires that the electron correlations suppress the inter-orbital hybridization. This has been stressed in the context of iron-based superconductors[158].

B.   "Flat" bands and electron correlations

In heavy fermion systems, the f electrons experience a large local Coulomb interaction U (including the Hubbard and Hund's coupling) and, in addition, their bare bandwidth W_f is small. The enhanced U/W_f is responsible for the strongly correlated nature of the f electron system.

In d electron systems, one may be able to use the crystalline lattice geometry to produce narrow bands and, thus, to engineer enhanced correlation effect. In recent years, this direction has been explored in a number of materials, including several Fe-based kagome-lattice materials[159,160]. While the focus has been on the identification of Weyl nodes in their magnetically ordered states, one can envision the "flat" bands to provide a setting for strong correlation physics that may bear some analogy with what has been so extensively studied in heavy fermion metals.

Beyond the standard correlated electron cases, twisted bilayer graphene has provided a synthetic setting for narrow bands and strong correlation physics. When two layers of graphene are twisted to special angles[161], moiré bands are formed with a small bandwidth W_{m}. Even though the p electrons have relatively small Coulomb repulsion, which is smaller still due to the spatially extended nature of the electronic states in the moiré bands, U/W_{m} can be drastically enhanced compared to their bare graphene counterpart. In practice, U/W_{m} in the "magic angle" twisted bilayer graphene is of order unity. The emergence of a dome of superconductivity[10,162,163], nematic correlations[164–166], and other phenomena establish these systems as a new play ground to explore strong correlation physics. The intertwining of correlations and topology adds a further layer of richness to the physics of these systems.

C.   Strong electron correlations boosted by other interactions

As discussed earlier for the heavy fermion case, strong correlations create sensitivity also to other interactions. For instance, phonon-boosting effects have been suggested for a number of unconventional superconductors. In FeSe, a dramatic enhancement of the superconducting gap-opening temperature—from $8\,\mathrm{K}$ in bulk FeSe to nearly $70\,\mathrm{K}$ when a single-unit-cell FeSe layer is grown on $SrTiO_3$[167]—was attributed in part to the coupling of electrons in FeSe to a phonon mode in $SrTiO_3$. This proposal has received support by

the appearance of strong shaddow bands (Fig. 6d)[168], and has triggered further work; for instance, recent theoretical work has suggested that the small-momentum electron-phonon interaction underlying the replica bands boosts but cannot trigger superconductivity in this system[169]. Whether phonons also boost superconductivity in other 2D systems is a topic of active debate[170].

Also photons may enhance electron interactions, an effect investigated using ultrafast pump–probe experiments with intense light pulses in different frequency ranges[171]. Such experiments have demonstrated transitions between (transient) phases, for instance insulator–metal or metal-superconductor transitions. Pioneering work on light-induced superconductivity on the non-superconducting stripe-ordered cuprate $La_{1.675}Eu_{0.2}Sr_{0.125}CuO_4$ revealed transiently enhanced interlayer tunneling only 1-2 ps after irradiation with an intense mid-infrared femtosecond pulse[172]. Very recently, evidence for metastable light-induced superconductivity was found, again in a stripe-ordered cuprate $La_{1.885}Ba_{0.115}CuO_4$[173] but also in K_3C_{60} (Fig. 6f)[174]. In the former, the effect was attributed to the melting of the stripe order, delocalizing halted electrons that then form Cooper pairs. In the latter, where the pump photon energy was at least one order of magnitude larger than the low temperature equilibrium superconducting gap, coupling of light with high-energy excitations, either molecular vibrations or collective electronic modes, was suggested.

D. Strong correlations and topological states

We have highlighted how heavy fermion metals display a rich variety of quantum phases. A tip of iceberg is now seen in metallic phases that are topological, particularly the Weyl-Kondo semimetal. The appearance of topological semimetals raises an intriguing question—how does electronic topology enrich strongly correlated electron physics? For example, do strongly correlated topological semimetals lead to new varieties of superconductors?

Conversely, the development of the Weyl-Kondo semimetal phase illustrates how strong correlations drive topological states. In realizing this phase, the Kondo effect cooperates not only with the spin-orbit coupling but also with the nonsymmorphic space group. This points to a general strategy, namely that strong correlations cooperate with space group symmetry in producing correlated topological states of matter. We expect much exploration to take place on this strategy in heavy fermion metals as well as in a variety of other strongly

correlated electron systems.

E. Wider contexts

Strongly correlated systems display amplified responses to external stimuli. A defining property of heavy fermion metals is the large effective mass of their charge carriers, which is typically enhanced from the noninteracting value by three orders of magnitude. The amplification occurs in response to external parameters such as magnetic field, pressure, or doping. For Weyl-Kondo semimetals, we have mentioned the giant responses of both thermodynamic and magnetotransport properties. This illustrates the extreme sensitivity that characterizes strongly correlated states of matter, which may be important for applications in quantum technology.

Finally, it is instructive to place the study of strongly correlated systems in the overall context of research in quantum materials and beyond. In quantum materials we let nature work for us and reveal new physics that may not have been conceived by our imagination. The corresponding models and concepts could then be studied by, e.g., cold atom[175], photonic[176], or gravity systems. For example, cold atom systems can be used to emulate bad metals and strange metals (Fig. 8f). The emulated states can then be used for measurements that are challenging to perform in quantum materials. A case in point are quantum entanglement properties, which are easier to measure in cold atom systems[177].

VII. SUMMARY AND OUTLOOK

We have surveyed the considerable recent developments on quantum phases and fluctuations produced by strong correlations, using heavy fermion metals as a platform. The focus has been on the particularly interesting situation where quantum criticality—frequently seen in these systems at the border of antiferromagnetic order—involves quantum fluctuations that go beyond the suppression of the Landau order parameter, in the form of a destruction of the static Kondo effect. Because the Kondo effect involves charge and spin, breaking it up does not only create local moments that can order but also entails an electron localization–delocalization transition. The associated quantum critical behavior continues to reveal new surprises, including dynamical scaling in the charge channel. Even though these systems

22

are metallic, the presence of local moments allows for frustration and dimensionality as new axes of tuning. Experiments have thus probed a considerable phase space, and the understanding of the discovered phases and fluctuations is guided by theoretical work on the global phase diagram. There has been considerable new development in this delineation, from the realization of a frustration-induced strange metal phase to the sequential localization–delocalization from entwined spin and orbital degrees of freedom.

Quantum critical fluctuations turn the electronic system soft, and may therefore nucleate new phases, with unconventional superconductivity as prime example. There has been much excitement about how the electronic localization–delocalization transition and the associated drastic Fermi surface transformation influences unconventional superconductivity. More generally, in the realm of emergent phases of metallic systems, recent studies seem to have seen a tip of iceberg in how strong correlations drive topological phases.

These developments set the stage for answering a set of fascinating outstanding questions that are pertinent to strongly correlated metals beyond the heavy fermion settings. We close the article by listing a few of them:

- How broadly relevant is the electronic localization–delocalization transition to strongly correlated electron systems? For instance, how to establish that the Fermi surface transformation observed in the high-T_c cuprates and other Mott-Hubbard systems reflects the amplified quantum fluctuations associated with electrons on the verge of localization? What are the pertinent tuning axes for an overall zero-temperature phase diagram that delineates the concurrence or detachment between the localization–delocalization transition and the development of electronic orders?

- We have hypothesized a strategy for strong correlations to produce topological states. In addition to the heavy fermion semimetals, what are the materials platforms that can be used to explore this strategy? Can an overall phase diagram be devised that delineates strong-correlation driven topological phases and classifies their fluctuations?

- The rich phenomena observed in strongly correlated materials comes with considerable complexity. When disentangled, it leads to new and much clearer understanding. How can synthetic platforms such as cold atom or mesoscopic systems be most efficiently used to elucidate the underlying simplicity?

- We have pointed out the extreme sensitivity of strongly correlated systems to external

stimuli and their giant responses, in particular if nontrivial topology is involved. Can this be exploited from quantum devices?

1. Badoux, S., Tabis, W., Laliberté, F., Grissonnanche, G., Vignolle, B., Vignolles, D., Béard, J., Bonn, D. A., Hardy, W. N., Liang, R., Doiron-Leyraud, N., Taillefer, L. & Proust, C. Change of carrier density at the pseudogap critical point of a cuprate superconductor. *Nature* **531**, 210 (2016).

2. Schröder, A., Aeppli, G., Coldea, R., Adams, M., Stockert, O., v. Löhneysen, H., Bucher, E., Ramazashvili, R. & Coleman, P. Onset of antiferromagnetism in heavy-fermion metals. *Nature* **407**, 351 (2000).

3. Paschen, S., Lühmann, T., Wirth, S., Gegenwart, P., Trovarelli, O., Geibel, C., Steglich, F., Coleman, P. & Si, Q. Hall-effect evolution across a heavy-fermion quantum critical point. *Nature* **432**, 881 (2004).

4. Shishido, H., Settai, R., Harima, H. & Onuki, Y. A drastic change of the Fermi surface at a critical pressure in CeRhIn$_5$: dHvA study under pressure. *J. Phys. Soc. Jpn.* **74**, 1103 (2005).

5. Friedemann, S., Oeschler, N., Wirth, S., Krellner, C., Geibel, C., Steglich, F., Paschen, S., Kirchner, S. & Si, Q. Fermi-surface collapse and dynamical scaling near a quantum-critical point. *Proc. Natl. Acad. Sci. U.S.A.* **107**, 14547 (2010).

6. Custers, J., Lorenzer, K., Müller, M., Prokofiev, A., Sidorenko, A., Winkler, H., Strydom, A. M., Shimura, Y., Sakakibara, T., Yu, R., Si, Q. & Paschen, S. Destruction of the Kondo effect in the cubic heavy-fermion compound Ce$_3$Pd$_{20}$Si$_6$. *Nat. Mater.* **11**, 189 (2012).

7. Prochaska, L., Li, X., MacFarland, D. C., Andrews, A. M., Bonta, M., Bianco, E. F., Yazdi, S., Schrenk, W., Detz, H., Limbeck, A., Si, Q., Ringe, E., Strasser, G., Kono, J. & Paschen, S. Singular charge fluctuations at a magnetic quantum critical point. *Science* **367**, 285 (2020).

8. Park, T., Ronning, F., Yuan, H. Q., Salamon, M. B., Movshovich, R., Sarrao, J. L. & Thompson, J. D. Hidden magnetism and quantum criticality in the heavy fermion superconductor CeRhIn$_5$. *Nature* **440**, 65 (2006).

9. Oike, H., Miyagawa, K., Taniguchi, H. & Kanoda, K. Pressure-induced Mott transition in an organic superconductor with a finite doping level. *Phys. Rev. Lett.* **114**, 067002 (2015).

10. Cao, Y., Fatemi, V., Fang, S., Watanabe, K., Taniguchi, T., Kaxiras, E. & Jarillo-Herrero, P. Unconventional superconductivity in magic-angle graphene superlattices. *Nature* **556**, 43 (2018).

11. Tokura, Y. & Nagaosa, N. Orbital physics in transition-metal oxides. *Science* **288**, 462 (2000).

12. Si, Q., Yu, R. & Abrahams, E. High-temperature superconductivity in iron pnictides and chalcogenides. *Nat. Rev. Mater.* **1**, 16017 (2016).

13. Kung, H.-H., Ran, S., Kanchanavatee, N., Krapivin, V., Lee, A., Mydosh, J. A., Haule, K., Maple, M. B. & Blumberg, G. Analogy between the "hidden order" and the orbital antiferromagnetism in $URu_{2-x}Fe_xSi_2$. *Phys. Rev. Lett.* **117**, 227601 (2016).

14. Martelli, V., Cai, A., Nica, E. M., Taupin, M., Prokofiev, A., Liu, C.-C., Lai, H.-H., Yu, R., Ingersent, K., Küchler, R., Strydom, A. M., Geiger, D., Haenel, J., Larrea, J., Si, Q. & Paschen, S. Sequential localization of a complex electron fluid. *Proc. Natl. Acad. Sci. U.S.A.* **116**, 17701 (2019).

15. Schaffer, R., Lee, E. K.-H., Yang, B.-J. & Kim, Y. B. Recent progress on correlated electron systems with strong spin-orbit coupling. *Rep. Prog. Phys.* **79**, 094504 (2016).

16. Savary, L. & Balents, L. Quantum spin liquids: a review. *Rep. Prog. Phys.* **80** (2017).

17. Zhou, Y., Kanoda, K. & Ng, T.-K. Quantum spin liquid states. *Rev. Mod. Phys.* **89**, 025003 (2017).

18. Dzsaber, S., Prochaska, L., Sidorenko, A., Eguchi, G., Svagera, R., Waas, M., Prokofiev, A., Si, Q. & Paschen, S. Kondo insulator to semimetal transformation tuned by spin-orbit coupling. *Phys. Rev. Lett.* **118**, 246601 (2017).

19. Lai, H.-H., Grefe, S. E., Paschen, S. & Si, Q. Weyl-Kondo semimetal in heavy-fermion systems. *Proc. Natl. Acad. Sci. U.S.A.* **115**, 93 (2018).

20. Stormer, H. L. Nobel lecture: The fractional quantum Hall effect. *Rev. Mod. Phys.* **71**, 875 (1999).

21. Wen, X.-G. Colloquium: Zoo of quantum-topological phases of matter. *Rev. Mod. Phys.* **89**, 041004 (2017).

22. Si, Q., Rabello, S., Ingersent, K. & Smith, J. Locally critical quantum phase transitions in strongly correlated metals. *Nature* **413**, 804 (2001).

23. Coleman, P., Pépin, C., Si, Q. & Ramazashvili, R. How do Fermi liquids get heavy and die? *J. Phys.: Condens. Matter* **13**, R723 (2001).

24. Senthil, T., Vojta, M. & Sachdev, S. Weak magnetism and non-Fermi liquids near heavy-fermion critical points. *Phys. Rev. B* **69**, 035111 (2004).

25. Keimer, B., Kivelson, S. A., Norman, M. R., Uchida, S. & Zaanen, J. From quantum matter to high-temperature superconductivity in copper oxides. *Nature* **518**, 179 (2015).

26. Si, Q. & Steglich, F. Heavy fermions and quantum phase transitions. *Science* **329**, 1161 (2010).

27. Hewson, A. C. *The Kondo Problem to Heavy Fermions* (Cambridge University Press, Cambridge, 1997).

28. Doniach, S. The Kondo lattice and weak antiferromagnetism. *Physica B+C* **91**, 231 (1977).

29. Stewart, G. R. Non-Fermi-liquid behavior in d- and f-electron metals. *Rev. Mod. Phys.* **73**, 797 (2001).

30. Coleman, P. & Schofield, A. J. Quantum criticality. *Nature* **433**, 226 (2005).

31. v. Löhneysen, H., Rosch, A., Vojta, M. & Wölfle, P. Fermi-liquid instabilities at magnetic quantum critical points. *Rev. Mod. Phys.* **79**, 1015 (2007).

32. Special Issue: Quantum Criticality and Novel Phases. *Phys. Status Solidi B* **250**, 417–659 (2013).

33. Si, Q. & Paschen, S. Quantum phase transitions in heavy fermion metals and Kondo insulators. *Phys. Status Solidi B* **250**, 425 (2013).

34. Kirchner, S., Paschen, S., Chen, Q., Wirth, S., Feng, D., Thompson, J. D. & Si, Q. Colloquium: Heavy-electron quantum criticality and single-particle spectroscopy. *Rev. Mod. Phys.* **92**, 011002 (2020).

35. Andres, K., Graebner, J. E. & Ott, H. R. $4f$-virtual-bound-state formation in $CeAl_3$ at low temperatures. *Phys. Rev. Lett.* **35**, 1779 (1975).

36. Kadowaki, K. & Woods, S. B. Universal relationship of the resistivity and specific heat in heavy-fermion compounds. *Solid State Commun.* **58**, 507 (1986).

37. Tsujii, N., Kontani, H. & Yoshimura, K. Universality in heavy fermion systems with general degeneracy. *Phys. Rev. Lett.* **94**, 057201 (2005).

38. Jacko, A. C., Fjaerestad, J. O. & Powell, B. J. A unified explanation of the Kadowaki–Woods ratio in strongly correlated metals. *Nat. Phys.* **5**, 422 (2009).

39. Zhu, L., Garst, M., Rosch, A. & Si, Q. Universally diverging Grüneisen parameter and the magnetocaloric effect close to quantum critical points. *Phys. Rev. Lett.* **91**, 066404 (2003).

40. Wu, J., Zhu, L. & Si, Q. Entropy accumulation near quantum critical points: effects beyond hyperscaling. *J. Phys. Conf. Ser.* **273**, 012019 (2011).

41. Keimer, B. & Moore, J. E. The physics of quantum materials. *Nat. Phys.* **13**, 1045 (2017).

42. Ball, P. Quantum materials: where many paths meet. *MRS Bulletin* **42**, 698 (2017).

43. Hussey, N. E., Takenaka, K. & Takagi, H. Universality of the Mott–Ioffe–Regel limit in metals. *Philos. Mag.* **84**, 2847 (2004).

44. Yi, M., Zhang, Y., Shen, Z.-X. & Lu, D. Role of the orbital degree of freedom in iron-based superconductors. *npj Quantum Materials* **2**, 57 (2017).

45. Dressel, M., Kasper, N., Petukhov, K., Peligrad, D. N., Gorshunov, B., Jourdan, M., Huth, M. & Adrian, H. Correlation gap in the heavy-fermion antiferromagnet UPd_2Al_3. *Phys. Rev. B* **66**, 035110 (2002).

46. Qazilbash, M. M., Hamlin, J. J., Baumbach, R. E., Zhang, L., Singh, D. J., Maple, M. B. & Basov, D. N. Electronic correlations in the iron pnictides. *Nat. Phys.* **5**, 647 (2009).

47. Yamamoto, S. & Si, Q. Fermi surface and antiferromagnetism in the Kondo Lattice: An asymptotically exact solution in $d > 1$ dimensions. *Phys. Rev. Lett.* **99**, 016401 (2007).

48. Gegenwart, P., Westerkamp, T., Krellner, C., Tokiwa, Y., Paschen, S., Geibel, C., Steglich, F., Abrahams, E. & Si, Q. Multiple energy scales at a quantum critical point. *Science* **315**, 969 (2007).

49. Seiro, S., Jiao, L., Kirchner, S., Hartmann, S., Friedemann, S., Krellner, C., Geibel, C., Si, Q., Steglich, F. & Wirth, S. Evolution of the Kondo lattice and non-Fermi liquid excitations in a heavy-fermion metal. *Nat. Commun.* **9**, 3324 (2018).

50. Hegger, H., Petrovic, C., Moshopoulou, E. G., Hundley, M. F., Sarrao, J. L., Fisk, Z. & Thompson, J. D. Pressure-induced superconductivity in quasi-2D $CeRhIn_5$. *Phys. Rev. Lett.* **84**, 4986 (2000).

51. Knebel, G., Aoki, D., Brison, J.-P. & Flouquet, J. The quantum critical point in $CeRhIn_5$: a resistivity study. *J. Phys. Soc. Jpn.* **77**, 114704 (2008).

52. Grempel, D. R. & Si, Q. Locally critical point in an anisotropic Kondo lattice. *Phys. Rev. Lett.* **91**, 026401 (2003).

53. Hu, H., Cai, A. & Si, Q. Quantum criticality and dynamical Kondo effect in an SU(2) Anderson lattice model. *arXiv:2004.04679* (2020).

54. Matsumoto, Y., Nakatsuji, S., Kuga, K., Karaki, Y., Horie, N., Shimura, Y., Sakakibara, T., Nevidomskyy, A. H. & Coleman, P. Quantum criticality without tuning in the mixed valence compound β-$YbAlB_4$. *Science* **331**, 316 (2011).

55. Hertz, J. A. Quantum critical phenomena. *Phys. Rev. B* **14**, 1165 (1976).

56. Millis, A. J. Effect of a nonzero temperature on quantum critical points in itinerant fermion systems. *Phys. Rev. B* **48**, 7183 (1993).

57. Moriya, T. *Spin fluctuations in itinerant electron magnetism*, vol. 56, 44–81 (Springer, Berlin, 1985).

58. Levin, K. & Valls, O. Phenomenological theories of liquid ^{3}He. *Phys. Rep.* **98**, 1 (1983).

59. Cai, A., Hu, H., Ingersent, K., Paschen, S. & Si, Q. Dynamical Kondo effect and Kondo destruction in effective models for quantum critical heavy fermion metals. *arXiv:1904.11471* (2019).

60. Nejati, A., Ballmann, K. & Kroha, J. Kondo destruction in RKKY-coupled Kondo lattice and multi-impurity systems. *Phys. Rev. Lett.* **118**, 117204 (2017).

61. Arndt, J., Stockert, O., Schmalzl, K., Faulhaber, E., Jeevan, H. S., Geibel, C., Schmidt, W., Loewenhaupt, M. & Steglich, F. Spin fluctuations in normal state CeCu$_2$Si$_2$ on approaching the quantum critical point. *Phys. Rev. Lett.* **106**, 246401 (2011).

62. Senthil, T., Vishwanath, A., Balents, L., Sachdev, S. & Fisher, M. Deconfined quantum critical points. *Science* **303**, 1490 (2004).

63. Zhu, L., Kirchner, S., Si, Q. & Georges, A. Quantum critical properties of the Bose-Fermi Kondo model in a large-N limit. *Phys. Rev. Lett.* **93**, 267201 (2004).

64. Komijani, Y. & Coleman, P. Emergent critical charge fluctuations at the Kondo breakdown of heavy fermions. *Phys. Rev. Lett.* **122**, 217001 (2019).

65. Cai, A., Yu, Z., Hu, H., Kirchner, S. & Si, Q. Dynamical scaling of charge and spin responses at a Kondo destruction quantum critical point. *Phys. Rev. Lett.* **124**, 027205 (2020).

66. Pixley, J. H., Chowdhury, T., Miecnikowski, M. T., Stephens, J., Wagner, C. & Ingersent, K. Entanglement entropy near Kondo-destruction quantum critical points. *Phys. Rev. B* **91**, 245122 (2015).

67. Wagner, C., Chowdhury, T., Pixley, J. H. & Ingersent, K. Long-range entanglement near a Kondo-destruction quantum critical point. *Phys. Rev. Lett.* **121**, 147602 (2018).

68. Mathur, N., Grosche, F., Julian, S., Walker, I., Freye, D., Haselwimmer, R. & Lonzarich, G. Magnetically mediated superconductivity in heavy fermion compounds. *Nature* **394**, 39 (1998).

69. Steglich, F. & Wirth, S. Foundations of heavy-fermion superconductivity: lattice Kondo

effect and Mott physics. *Rep. Prog. Phys.* **79**, 084502 (2016).

70. Scalapino, D. J. A common thread: The pairing interaction for unconventional superconductors. *Rev. Mod. Phys.* **84**, 1383 (2012).

71. Pixley, J. H., Deng, L., Ingersent, K. & Si, Q. Pairing correlations near a Kondo-destruction quantum critical point. *Phys. Rev. B* **91**, 201109 (2015).

72. Cai, A., Pixley, J. H., Ingersent, K. & Si, Q. Critical local moment fluctuations and enhanced pairing correlations in a cluster Anderson model. *Phys. Rev. B* **101**, 014452 (2020).

73. Steglich, F., Aarts, J., Bredl, C. D., Lieke, W., Meschede, D., Franz, W. & Schäfer, H. Superconductivity in the presence of strong Pauli paramagnetism: CeCu$_2$Si$_2$. *Phys. Rev. Lett.* **43**, 1892 (1979).

74. Stockert, O., Arndt, J., Faulhaber, E., Geibel, C., Jeevan, . H. S., Kirchner, S., Loewenhaupt, M., Schmalzl, K., Schmidt, W., Si, Q. . & Steglich, F. Magnetically driven superconductivity in CeCu$_2$Si$_2$. *Nat. Phys.* **7**, 119 (2011).

75. Stock, C., Broholm, C., Hudis, J., Kang, H. J. & Petrovic, C. Spin resonance in the *d*-wave superconductor CeCoIn$_5$. *Phys. Rev. Lett.* **100**, 087001 (2008).

76. Stockert, O., Kirchner, S., Steglich, F. & Si, Q. Superconductivity in Ce- and U-based '122' heavy-fermion compounds. *J. Phys. Soc. Jpn.* **81**, 011001 (2012).

77. Nica, E. M., Yu, R. & Si, Q. Orbital-selective pairing and superconductivity in iron selenides. *npj Quantum Materials* **2**, 24 (2017).

78. Nica, E. M. & Si, Q. Multiorbital singlet pairing and *d+d* superconductivity. *arXiv:1911.13274* (2019).

79. Pang, G., Smidman, M., Zhang, J., Jiao, L., Weng, Z., Nica, E. M., Chen, Y., Jiang, W., Zhang, Y., Xie, W., Jeevan, H. S., Lee, H., Gegenwart, P., Steglich, F., Si, Q. & Yuan, H. Fully gapped d-wave superconductivity in CeCu$_2$Si$_2$. *Proc. Natl. Acad. Sci. U.S.A.* **115**, 5343 (2018).

80. Yamashita, T., Takenaka, T., Tokiwa, Y., Wilcox, J. A., Mizukami, Y., Terazawa, D., Kasahara, Y., Kittaka, S., Sakakibara, T., Konczykowski, M., Seiro, S., Jeevan, H. S., Geibel, C., Putzke, C., Onishi, T., Ikeda, H., Carrington, A., Shibauchi, T. & Matsuda, Y. Fully gapped superconductivity with no sign change in the prototypical heavy-fermion CeCu$_2$Si$_2$. *Sci. Adv.* **3** (2017).

81. Kittaka, S., Aoki, Y., Shimura, Y., Sakakibara, T., Seiro, S., Geibel, C., Steglich, F., Ikeda,

H. & Machida, K. Multiband superconductivity with unexpected deficiency of nodal quasi-particles in $CeCu_2Si_2$. *Phys. Rev. Lett.* **112**, 067002 (2014).

82. Smidman, M., Stockert, O., Arndt, J., Pang, G. M., Jiao, L., Yuan, H. Q., Vieyra, H. A., Kitagawa, S., Ishida, K., Fujiwara, K., Kobayashi, T. C., Schuberth, E., Tippmann, M., Steinke, L., Lausberg, S., Steppke, A., Brando, M., Pfau, H., Stockert, U., Sun, P., Friedemann, S., Wirth, S., Krellner, C., Kirchner, S., Nica, E. M., Yu, R., Si, Q. & Steglich, F. Interplay between unconventional superconductivity and heavy-fermion quantum criticality: $CeCu_2Si_2$ versus $YbRh_2Si_2$. *Philos. Mag.* **98**, 2930 (2018).

83. Ikeda, H., Suzuki, M.-T. & Arita, R. Emergent loop-nodal $s_\pm$-wave superconductivity in $CeCu_2Si_2$: Similarities to the iron-based superconductors. *Phys. Rev. Lett.* **114**, 147003 (2015).

84. Li, Y., Liu, M., Fu, Z., Chen, X., Yang, F. & Yang, Y.-f. Gap symmetry of the heavy fermion superconductor $CeCu_2Si_2$ at ambient pressure. *Phys. Rev. Lett.* **120**, 217001 (2018).

85. Schuberth, E., Tippmann, M., Steinke, L., Lausberg, S., Steppke, A., Brando, M., Krellner, C., Geibel, C., Yu, R., Si, Q. & Steglich, F. Emergence of superconductivity in the canonical heavy-electron metal $YbRh_2Si_2$. *Science* **351**, 485 (2016).

86. Jiao, L., Chen, Y., Kohama, Y., Graf, D., Bauer, E. D., Singleton, J., Zhu, J.-X., Weng, Z., Pang, G., Shang, T., Zhang, J., Lee, H.-O., Park, T., Jaime, M., Thompson, J. D., Steglich, F., Si, Q. & Yuan, H. Q. Fermi surface reconstruction and multiple quantum phase transitions in the antiferromagnet $CeRhIn_5$. *Proc. Natl. Acad. Sci. U.S.A.* **112**, 673 (2015).

87. Ronning, F., Helm, T., Hirer, K. R. S., Bachmann, M. D., Balicas, L., Chan, M. K., Ramshaw, B. J., McDonald, R. D., Balakirev, F. F., Jaime, M., Bauer, E. D. & Moll, P. J. W. Electronic in-plane symmetry breaking at field-tuned quantum criticality in $CeRhIn_5$. *Nature* **548**, 313 (2017).

88. Nisoli, C., Moessner, R. & Schiffer, P. Colloquium: Artificial spin ice: Designing and imaging magnetic frustration. *Rev. Mod. Phys.* **85**, 1473 (2013).

89. Si, Q. Global magnetic phase diagram and local quantum criticality in heavy fermion metals. *Physica B* **378-380**, 23 (2006).

90. Si, Q. Quantum criticality and global phase diagram of magnetic heavy fermions. *Phys. Status Solidi B* **247**, 476 (2010).

91. Coleman, P. & Nevidomskyy, A. Frustration and the Kondo effect in heavy fermion materials.

J. Low Temp. Phys. **161**, 182 (2010).

92. Vojta, M. From itinerant to local-moment antiferromagnetism in Kondo lattices: Adiabatic continuity versus quantum phase transitions. *Phys. Rev. B* **78**, 125109 (2008).

93. Pixley, J. H., Yu, R. & Si, Q. Quantum phases of the Shastry-Sutherland Kondo lattice: Implications for the global phase diagram of heavy-fermion metals. *Phys. Rev. Lett.* **113**, 176402 (2014).

94. Sato, T., Assaad, F. F. & Grover, T. Quantum Monte Carlo simulation of frustrated Kondo lattice models. *Phys. Rev. Lett.* **120**, 107201 (2018).

95. Kurita, N., Yamamoto, D., Kanesaka, T., Furukawa, N., Ohira-Kawamura, S., Nakajima, K. & Tanaka, H. Localized magnetic excitations in the fully frustrated dimerized magnet $Ba_2CoSi_2O_6Cl_2$. *Phys. Rev. Lett.* **123**, 027206 (2019).

96. Li, B., Yan, J.-Q., Pajerowski, D. M., Gordon, E., Nedic, A.-M., Sizyuk, Y., Ke, L., Orth, P. P., Vaknin, D. & McQueeney, R. J. Competing magnetic interactions in the antiferromagnetic topological insulator $MnBi_2Te_4$. *Phys. Rev. Lett.* **124**, 167204 (2020).

97. Nakatsuji, S., Machida, Y., Maeno, Y., Tayama, T., Sakakibara, T., van Duijn, J., Balicas, L., Millican, J. N., Macaluso, R. T. & Chan, J. Y. Metallic spin-liquid behavior of the geometrically frustrated Kondo lattice $Pr_2Ir_2O_7$. *Phys. Rev. Lett.* **96**, 087204 (2006).

98. Kim, M. S. & Aronson, M. C. Heavy fermion compounds on the geometrically frustrated Shastry-Sutherland lattice. *J. Phys.: Condens. Matter* **23**, 164204 (2011).

99. Fritsch, V., Bagrets, N., Goll, G., Kittler, W., Wolf, M. J., Grube, K., Huang, C.-L. & Löhneysen, H. v. Approaching quantum criticality in a partially geometrically frustrated heavy-fermion metal. *Phys. Rev. B* **89**, 054416 (2014).

100. Tokiwa, Y., Stingl, C., Kim, M.-S., Takabatake, T. & Gegenwart, P. Characteristic signatures of quantum criticality driven by geometrical frustration. *Sci. Adv.* **1**, e1500001 (2015).

101. Wu, L. S., Gannon, W. J., Zaliznyak, I. A., Tsvelik, A. M., Brockmann, M., Caux, J.-S., Kim, M. S., Qiu, Y., Copley, J. R. D., Ehlers, G., Podlesnyak, A. & Aronson, M. C. Orbital-exchange and fractional quantum number excitations in an f-electron metal, Yb_2Pt_2Pb. *Science* **352**, 1206 (2016).

102. Zhao, H., Zhang, J., Lyu, M., Bachus, S., Tokiwa, Y., Gegenwart, P., Zhang, S., Cheng, J., Yang, Y.-f., Chen, G., Isikawa, Y., Si, Q., Steglich, F. & Sun, P. Quantum-critical phase from frustrated magnetism in a strongly correlated metal. *Nat. Phys.* **15**, 1261 (2019).

103. Kavai, M., Friedman, J., Sherman, K., Gong, M., Giannakis, I., Hajinazar, S., Hu, H., Grefe, S. E., Leshen, J., Yang, Q., Nakatsuji, S., Kolmogorov, A. N., Si, Q., Lawler, M. & Aynajian, P. Discovery of nanoscale phase coexistence of heavy Fermi-liquid and metallic spin-liquid in geometrically frustrated $Pr_2Ir_2O_7$. *arXiv:2006.07424* (2020).

104. Stockert, O., Hoffmann, J.-U., Mühlbauer, M., Senyshyn, A., Koza, M. M., Tsirlin, A. A., Wolf, F. M., Bachus, S., Gegenwart, P., Movshovich, R., Bobev, S. & Fritsch, V. Magnetic frustration in a metallic fcc lattice. *Phys. Rev. Research* **2**, 013183 (2020).

105. Tokiwa, Y., Ishikawa, J. J., Nakatsuji, S. & Gegenwart, P. Quantum criticality in a metallic spin liquid. *Nat. Mater.* **13**, 356 (2014).

106. Küchler, R., Stingl, C., Tokiwa, Y., Kim, M. S., Takabatake, T. & Gegenwart, P. Uniaxial stress tuning of geometrical frustration in a Kondo lattice. *Phys. Rev. B* **96**, 241110 (2017).

107. Friedemann, S., Westerkamp, T., Brando, M., Oeschler, N., Wirth, S., Gegenwart, P., Krellner, C., Geibel, C. & Steglich, F. Detaching the antiferromagnetic quantum critical point from the Fermi-surface reconstruction in $YbRh_2Si_2$. *Nat. Phys.* **5**, 465 (2009).

108. Custers, J., Gegenwart, P., Geibel, C., Steglich, F., Coleman, P. & Paschen, S. Evidence for a non-Fermi-liquid phase in Ge-substituted $YbRh_2Si_2$. *Phys. Rev. Lett.* **104**, 186402 (2010).

109. Shishido, H., Shibauchi, T., Yasu, K., Kato, T., Kontani, H., Terashima, T. & Matsuda, Y. Tuning the dimensionality of the heavy fermion compound $CeIn_3$. *Science* **327**, 980 (2010).

110. Ishii, T., Toda, R., Hanaoka, Y., Tokiwa, Y., Shimozawa, M., Kasahara, Y., Endo, R., Terashima, T., Nevidomskyy, A. H., Shibauchi, T. & Matsuda, Y. Tuning the magnetic quantum criticality of artificial Kondo superlattices $CeRhIn_5/YbRhIn_5$. *Phys. Rev. Lett.* **116**, 206401 (2016).

111. Takabayashi, Y., Ganin, A. Y., Jeglič, P., Arčon, D., Takano, T., Iwasa, Y., Ohishi, Y., Takata, M., Takeshita, N., Prassides, K. & Rosseinsky, M. J. The disorder-free non-BCS superconductor Cs_3C_{60} emerges from an antiferromagnetic insulator parent state. *Science* **323**, 1585 (2009).

112. Ramshaw, B. J., Sebastian, S. E., McDonald, R. D., Day, J., Tan, B. S., Zhu, Z., Betts, J. B., Liang, R., Bonn, D. A., Hardy, W. N. & Harrison, N. Quasiparticle mass enhancement approaching optimal doping in a high-T_c superconductor. *Science* **348**, 317 (2015).

113. Hewson, A. C. & Meyer, D. Numerical renormalization group study of the Anderson-Holstein impurity model. *J. Phys.: Condens. Matter* **10**, 196401 (2002).

114. Lüffe, M. C., Koch, J. & von Oppen, F. Theory of vibrational absorption sidebands in the coulomb-blockade regime of single-molecule transistors. *Phys. Rev. B* **77**, 125306 (2008).

115. Kalla, M., Chebrolu, N. R. & Chatterjee, A. Magneto-transport properties of a single molecular transistor in the presence of electron-electron and electron-phonon interactions and quantum dissipation. *Sci. Rep.* **9**, 16510 (2019).

116. Hotta, T. Enhanced Kondo effect in an electron system dynamically coupled with local optical phonons. *J. Phys. Soc. Jpn.* **76**, 084702 (2007).

117. Prokofiev, A., Sidorenko, A., Hradil, K., Ikeda, M., Svagera, R., Waas, M., Winkler, H., Neumaier, K. & Paschen, S. Thermopower enhancement by encapsulating cerium in clathrate cages. *Nat. Mater.* **12**, 1096 (2013).

118. Haldane, F. Nobel Lecture: Topological quantum matter. *Rev. Mod. Phys.* **89**, 040502 (2017).

119. Hasan, M. Z. & Kane, C. L. Colloquium: Topological insulators. *Rev. Mod. Phys.* **82**, 3045 (2010).

120. Qi, X.-L. & Zhang, S.-C. Topological insulators and superconductors. *Rev. Mod. Phys.* **83**, 1057 (2011).

121. Focus Issue "Topological semimetals". Nat. Mater. **15**, No. 11 (2016).

122. Bansil, A., Lin, H. & Das, T. Colloquium: Topological band theory. *Rev. Mod. Phys.* **88**, 021004 (2016).

123. Armitage, N. P., Mele, E. J. & Vishwanath, A. Weyl and Dirac semimetals in three-dimensional solids. *Rev. Mod. Phys.* **90**, 015001 (2018).

124. Chiu, C.-K., Teo, J. C. Y., Schnyder, A. P. & Ryu, S. Classification of topological quantum matter with symmetries. *Rev. Mod. Phys.* **88**, 035005 (2016).

125. Po, H. C., Vishwanath, A. & Watanabe, H. Symmetry-based indicators of band topology in the 230 space groups. *Nat. Commun.* **8**, 50 (2017).

126. Zhang, T., Jiang, Y., Song, Z., Huang, H., He, Y., Fang, Z., Weng, H. & Fang, C. Catalogue of topological electronic materials. *Nature* **566**, 475 (2019).

127. Vergniory, M. G., Elcoro, L., Felser, C., Regnault, N., Bernevig, B. A. & Wang, Z. A complete catalogue of high-quality topological materials. *Nature* **566**, 480 (2019).

128. Tang, F., Po, H. C., Vishwanath, A. & Wan, X. Comprehensive search for topological materials using symmetry indicators. *Nature* **566**, 486 (2019).

129. Frantzeskakis, E., Ramankutty, S. V., de Jong, N., Huang, Y. K., Pan, Y., Tytarenko, A.,

Radovic, M., Plumb, N. C., Shi, M., Varykhalov, A., de Visser, A., van Heumen, E. & Golden, M. S. Trigger of the ubiquitous surface band bending in 3D topological insulators. *Phys. Rev. X* **7**, 041041 (2017).

130. Huang, X., Zhao, L., Long, Y., Wang, P., Chen, D., Yang, Z., Liang, H., Xue, M., Weng, H., Fang, Z., Dai, X. & Chen, G. Observation of the chiral-anomaly-induced negative magnetoresistance in 3D Weyl semimetal TaAs. *Phys. Rev. X* **5**, 031023 (2015).

131. Moll, P. J. W., Nair, N. L., Helm, T., Potter, A. C., Kimchi, I., Vishwanath, A. & Analytis, J. G. Transport evidence for Fermi-arc-mediated chirality transfer in the Dirac semimetal Cd_3As_2. *Nature* **535**, 266 (2016).

132. Zhang, C.-L., Xu, S.-Y., Belopolski, I., Yuan, Z., Lin, Z., Tong, B., Bian, G., Alidoust, N., Lee, C.-C., Huang, S.-M., Chang, T.-R., Chang, G., Hsu, C.-H., Jeng, H.-T., Neupane, M., Sanchez, D. S., Zheng, H., Wang, J., Lin, H., Zhang, C., Lu, H.-Z., Shen, S.-Q., Neupert, T., Zahid Hasan, M. & Jia, S. Signatures of the Adler–Bell–Jackiw chiral anomaly in a Weyl fermion semimetal. *Nat. Commun.* **7**, 10735 (2016).

133. Zhang, C., Zhang, Y., Yuan, X., Lu, S., Zhang, J., Narayan, A., Liu, Y., Zhang, H., Ni, Z., Liu, R., Choi, E. S., Suslov, A., Sanvito, S., Pi, L., Lu, H.-Z., Potter, A. C. & Xiu, F. Quantum Hall effect based on Weyl orbits in Cd_3As_2. *Nature* **565**, 331 (2019).

134. Shao, Y., Rudenko, A. N., Hu, J., Sun, Z., Zhu, Y., Moon, S., Millis, A. J., Yuan, S., Lichtenstein, A. I., Smirnov, D., Mao, Z. Q., Katsnelson, M. I. & Basov, D. N. Electronic correlations in nodal-line semimetals. *Nat. Phys.* **16**, 636 (2020).

135. Tang, H.-K., Leaw, J. N., Rodrigues, J. N. B., Herbut, I. F., Sengupta, P., Assaad, F. F. & Adam, S. The role of electron-electron interactions in two-dimensional dirac fermions. *Science* **361**, 570 (2018).

136. Grefe, S. E., Lai, H.-H., Paschen, S. & Si, Q. Weyl-Kondo semimetals in nonsymmorphic systems. *Phys. Rev. B* **101**, 075138 (2020).

137. Dzsaber, S., Yan, X., Eguchi, G., Prokofiev, A., Shiroka, T., Blaha, P., Rubel, O., Grefe, S. E., Lai, H.-H., Si, Q. & Paschen, S. Giant spontaneous Hall effect in a nonmagnetic Weyl-Kondo semimetal. *arXiv:1811.02819* (2018).

138. Dzsaber, S., Zocco, D. A., McCollam, A., Weickert, F., McDonald, R., Taupin, M., Yan, X., Prokofiev, A., Tang, L. M. K., Vlaar, B., Stritzinger, L., Jaime, M., Si, Q. & Paschen, S. Quenching a Weyl-Kondo semimetal by magnetic field. *arXiv:1906.01182* (2019).

139. Guo, C., Cao, C., Smidman, M., Wu, F., Zhang, Y., Steglich, F., Zhang, F.-C. & Yuan, H. Possible Weyl fermions in the magnetic Kondo system CeSb. *npj Quantum Materials* **2**, 39 (2017).

140. Guo, C. Y., Wu, F., Wu, Z. Z., Smidman, M., Cao, C., Bostwick, A., Jozwiak, C., Rotenberg, E., Liu, Y., Steglich, F. & Yuan, H. Q. Evidence for Weyl fermions in a canonical heavy-fermion semimetal YbPtBi. *Nat. Commun.* **9**, 4622 (2018).

141. Schoop, L. M., Topp, A., Lippmann, J., Orlandi, F., Müchler, L., Vergniory, M. G., Sun, Y., Rost, A. W., Duppel, V., Krivenkov, M., Sheoran, S., Manuel, P., Varykhalov, A., Yan, B., Kremer, R. K., Ast, C. R. & Lotsch, B. V. Tunable Weyl and Dirac states in the nonsymmorphic compound CeSbTe. *Sci. Adv.* **4**, eaar2317 (2018).

142. Zhai, L.-J., Chou, P.-H. & Mou, C.-Y. Magnetic phases and unusual topological electronic structures of weyl semimetals in strong interaction limit. *Phys. Rev. B* **94**, 125135 (2016).

143. Xu, Y., Yue, C., Weng, H. & Dai, X. Heavy Weyl fermion state in CeRu$_4$Sn$_6$. *Phys. Rev. X* **7**, 011027 (2017).

144. Roy, B., Goswami, P. & Juričić, V. Interacting Weyl fermions: Phases, phase transitions, and global phase diagram. *Phys. Rev. B* **95**, 201102 (2017).

145. Chang, P.-Y. & Coleman, P. Parity-violating hybridization in heavy Weyl semimetals. *Phys. Rev. B* **97**, 155134 (2018).

146. Ivanov, V., Wan, X. & Savrasov, S. Y. Topological insulator-to-Weyl semimetal transition in strongly correlated actinide system UNiSn. *Phys. Rev. X* **9**, 041055 (2019).

147. Lu, Y.-W., Chou, P.-H., Chung, C.-H. & Mou, C.-Y. Tunable topological semimetallic phases in Kondo lattice systems. *Phys. Rev. B* **99**, 035141 (2019).

148. Wang, L.-J., Hu, X.-T., Li, L., Xu, D.-H., Sun, J.-H. & Chen, W.-Q. Spatial anisotropy of the Kondo screening cloud in a type-II Weyl semimetal. *Phys. Rev. B* **99**, 235108 (2019).

149. Yang, Y.-Y., Deng, M.-X., Duan, H.-J., Luo, W. & Wang, R.-Q. Electrically tunable Kondo effect as a direct measurement of the chiral anomaly in disordered Weyl semimetals. *Phys. Rev. B* **101**, 205137 (2020).

150. Grefe, S. E., Lai, H.-H., Paschen, S. & Si, Q. Weyl-Kondo semimetal: towards control of Weyl nodes. *JPS Conf. Proc.* **30**, 011013 (2020).

151. Joshi, D., Li, C., Tarnopolsky, G., Georges, A. & Sachdev, S. Deconfined critical point in a doped random quantum Heisenberg magnet. *arXiv:1912.08822* (2019).

152. Cha, P., Wentzell, N., Parcollet, O., Georges, A. & Kim, E. Linear resistivity and Sachdev-Ye-Kitaev (SYK) spin liquid behavior in a quantum critical metal with spin-1/2 fermions. *arXiv:2002.07181* (2020).

153. Senthil, T. Critical Fermi surfaces and non-Fermi liquid metals. *Phys. Rev. B* **78**, 035103 (2008).

154. Terletska, H., Vučičević, J., Tanasković, D. & Dobrosavljević, V. Quantum critical transport near the Mott transition. *Phys. Rev. Lett.* **107**, 026401 (2011).

155. Jia, Y., Gong, C., Liu, Y., Zhao, J., Dong, C., Dai, G., Li, X., Lei, H., Yu, R., Zhang, G. & Jin, C. Mott transition and superconductivity in quantum spin liquid candidate $NaYbSe_2$; *arXiv:2003.09859* (2020).

156. Pépin, C. Selective Mott transition and heavy fermions. *Phys. Rev. B* **77**, 245129 (2008).

157. Anisimov, V., Nekrasov, I., Kondakov, D., Rice, T. & Sigrist, M. Orbital-selective Mott-insulator transition in $Ca_{2-x}Sr_xRuO_4$. *Eur. Phys. J. B* **25**, 191 (2002).

158. Yu, R. & Si, Q. Orbital-selective Mott phase in multiorbital models for iron pnictides and chalcogenides. *Phys. Rev. B* **96**, 125110 (2017).

159. Kang, M., Ye, L., Fang, S., You, J.-S., Levitan, A., Han, M., Facio, J. I., Jozwiak, C., Bostwick, A., Rotenberg, E., Chan, M. K., McDonald, R. D., Graf, D., Kaznatcheev, K., Vescovo, E., Bell, D. C., Kaxiras, E., van den Brink, J., Richter, M., Prasad Ghimire, M., Checkelsky, J. G. & Comin, R. Dirac fermions and flat bands in the ideal kagome metal FeSn. *Nat. Mater.* **19**, 163 (2020).

160. Yao, M., Lee, H., Xu, N., Wang, Y., Ma, J., Yazyev, O., Xiong, Y., Shi, M., Aeppli, G. & Soh, Y. Switchable Weyl nodes in topological Kagome ferromagnet Fe_3Sn_2. *arXiv:1810.01514* (2018).

161. Bistritzer, R. & MacDonald, A. H. Moiré bands in twisted double-layer graphene. *Proc. Natl. Acad. Sci. U.S.A.* **108**, 12233 (2011).

162. Yankowitz, M., Chen, S., Polshyn, H., Zhang, Y., Watanabe, K., Taniguchi, T., Graf, D., Young, A. F. & Dean, C. R. Tuning superconductivity in twisted bilayer graphene. *Science* **363**, 1059 (2019).

163. Lu, X., Stepanov, P., Yang, W., Xie, M., Aamir, M. A., Das, I., Urgell, C., Watanabe, K., Taniguchi, T., Zhang, G., Bachtold, A., MacDonald, A. H. & Efetov, D. K. Superconductors, orbital magnets and correlated states in magic-angle bilayer graphene. *Nature* **574**, 653

(2019).

164. Kerelsky, A., McGilly, L. J., Kennes, D. M., Xian, L., Yankowitz, M., Chen, S., Watanabe, K., Taniguchi, T., Hone, J., Dean, C., Rubio, A. & Pasupathy, A. N. Maximized electron interactions at the magic angle in twisted bilayer graphene. *Nature* **572**, 95 (2019).

165. Choi, Y., Kemmer, J., Peng, Y., Thomson, A., Arora, H., Polski, R., Zhang, Y., Ren, H., Alicea, J., Refael, G., von Oppen, F., Watanabe, K., Taniguchi, T. & Nadj-Perge, S. Electronic correlations in twisted bilayer graphene near the magic angle. *Nat. Phys.* **15**, 1174 (2019).

166. Chen, L., Hu, H. & Si, Q. Fragile insulator and electronic nematicity in a graphene moiré system. *arXiv:2007.06086* (2020).

167. Wang, Q.-Y., Li, Z., Zhang, W.-H., Zhang, Z.-C., Zhang, J.-S., Li, W., Ding, H., Ou, Y.-B., Deng, P., Chang, K., Wen, J., Song, C.-L., He, K., Jia, J.-F., Ji, S.-H., Wang, Y.-Y., Wang, L.-L., Chen, X., Ma, X.-C. & Xue, Q.-K. Interface-induced high-temperature superconductivity in single unit-cell FeSe films on SrTiO$_3$. *Chin. Phys. Lett.* **29**, 037402 (2012).

168. Lee, J. J., Schmitt, F. T., Moore, R. G., Johnston, S., Cui, Y.-T., Moore, R. G., Johnston, S., Cui, Y.-T., Li, W., Yi, M., Liu, Z. K., Hashimoto, M., Zhang, Y., Lu, D. H., Devereaux, T. P., Lee, D.-H. & Shen, Z.-X. Interfacial mode coupling as the origin of the enhancement of T_c in FeSe films on SrTiO$_3$. *Nature* **515**, 245 (2014).

169. Li, Z.-X., Devereaux, T. P. & Lee, D.-H. Electronic and phononic properties of a two-dimensional electron gas coupled to dipolar phonons via small-momentum-transfer scattering. *Phys. Rev. B* **100** (2019).

170. Polshyn, H., Yankowitz, M., Chen, S., Zhang, Y., Watanabe, K., Taniguchi, T., Dean, C. R. & Young, A. F. Large linear-in-temperature resistivity in twisted bilayer graphene. *Nat. Phys.* **15**, 1011 (2019).

171. Giannetti, C., Capone, M., Fausti, D., Fabrizio, M., Parmigiani, F. & Mihailovic, D. Ultrafast optical spectroscopy of strongly correlated materials and high-temperature superconductors: a non-equilibrium approach. *Adv. Phys.* **65**, 58 (2016).

172. Fausti, D., Tobey, R. I., Dean, N., Kaiser, S., Dienst, A., Hoffmann, M. C., Pyon, S., Takayama, T., Takagi, H. & Cavalleri, A. Light-induced superconductivity in a stripe-ordered cuprate. *Science* **331**, 189 (2011).

173. Cremin, K. A., Zhang, J., Homes, C. C., Gu, G. D., Sun, Z., Fogler, M. M., Millis, A. J., Basov, D. N. & Averitt, R. D. Photoenhanced metastable c-axis electrodynamics in stripe-

ordered cuprate $La_{1.885}Ba_{0.115}CuO_4$. *Proc. Natl. Acad. Sci. U.S.A.* **116**, 19875 (2019).

174. M. Budden, T. Gebert, M. Buzzi, G. Jotzu, E. Wang, T. Matsuyama, G. Meier, Y. Laplace, D. Pontiroli, M. Riccò, F. Schlawin, D. Jaksch, and A. Cavalleri. Evidence for metastable photo-induced superconductivity in K_3C_{60}, *arXiv:2002.12835* (2020).

175. Brown, P. T., Mitra, D., Guardado-Sanchez, E., Nourafkan, R., Reymbaut, A., Hébert, C.-D., Bergeron, S., Tremblay, A.-M. S., Kokalj, J., Huse, D. A., Schauß, P. & Bakr, W. S. Bad metallic transport in a cold atom Fermi-Hubbard system. *Science* **363**, 379 (2019).

176. Ozawa, T., Price, H. M., Amo, A., Goldman, N., Hafezi, M., Lu, L., Rechtsman, M. C., Schuster, D., Simon, J., Zilberberg, O. & Carusotto, I. Topological photonics. *Rev. Mod. Phys.* **91**, 015006 (2019).

177. Islam, R., Ma, R., Preiss, P. M., Eric Tai, M., Lukin, A., Rispoli, M. & Greiner, M. Measuring entanglement entropy in a quantum many-body system. *Nature* **528**, 77 (2015).

178. Gegenwart, P., Custers, J., Geibel, C., Neumaier, K., Tayama, T., Tenya, K., Trovarelli, O. & Steglich, F. Magnetic-field induced quantum critical point in $YbRh_2Si_2$. *Phys. Rev. Lett.* **89**, 056402 (2002).

179. Sun, J. P., Matsuura, G. Z., K. Ye, Mizukami, Y., Shimozawa, M., Matsubayashi, K., Yamashita, M., Watashige, T., Kasahara, S., Matsuda, Y., Yan, J. Q., Sales, B. C., Uwatoko, Y., Cheng, J. G. & Shibauchi, T. Dome-shaped magnetic order competing with high-temperature superconductivity at high pressures in FeSe. *Nat. Commun.* **7**, 12146 (2016).

180. Nielsen, H. B. & Ninomiya, M. The Adler-Bell-Jackiw anomaly and Weyl fermions in a crystal. *Phys. Lett. B* **130**, 389 (1983).

181. Young, S. M., Zaheer, S., Teo, J. C. Y., Kane, C. L., Mele, E. J. & Rappe, A. M. Dirac semimetal in three dimensions. *Phys. Rev. Lett.* **108**, 140405 (2012).

182. Cano, J., Bradlyn, B., Wang, Z., Elcoro, L., Vergniory, M. G., Felser, C., Aroyo, M. I. & Bernevig, B. A. Building blocks of topological quantum chemistry: Elementary band representations. *Phys. Rev. B* **97**, 035139 (2018).

183. Xia, Y., Qian, D., Hsieh, D., Wray, L., Pal, A., Lin, H., Bansil, A., Grauer, D., Hor, Y. S., Cava, R. J. & Hasan, M. Z. Observation of a large-gap topological-insulator class with a single Dirac cone on the surface. *Nature Phys.* **5**, 398 (2009).

184. Liu, Z. K., Zhou, B., Zhang, Y., Wang, Z. J., Weng, H. M., Prabhakaran, D., Mo, S.-K., Shen, Z. X., Fang, Z., Dai, X., Hussain, Z. & Chen, Y. L. Discovery of a three-dimensional

topological Dirac semimetal, Na$_3$Bi. *Science* **343**, 864 (2014).

185. Xu, S.-Y., Belopolski, I., Alidoust, N., Neupane, M., Bian, G., Zhang, C., Sankar, R., Chang, G., Yuan, Z., Lee, C.-C., Huang, S.-M., Zheng, H., Ma, J., Sanchez, D. S., Wang, B., Bansil, A., Chou, F., Shibayev, P. P., Lin, H., Jia, S. & Hasan, M. Z. Discovery of a Weyl fermion semimetal and topological Fermi arcs. *Science* **349**, 613 (2015).
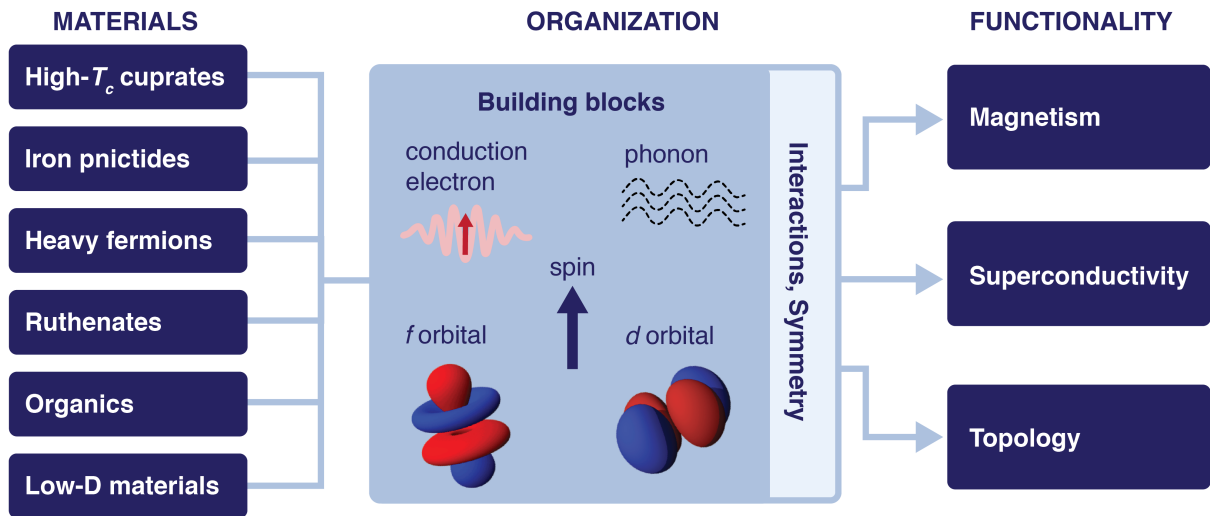
FIG. 1: **Functionality of strongly correlated materials.** Selected classes of strongly correlated materials, and how interactions between their low-energy degrees of freedom ("building blocks") and symmetry may lead to different functionalities. Examples of the rich resulting phase diagrams for several of these materials classes are shown in Fig. S1.

FIG. 2: **Tuning correlation strength. a**| Generalized Kadowaki-Woods plot, adapted with permission from ref. 37 to include ranges of A coefficient reached in experiments on the heavy fermion compounds $YbRh_2Si_2$ from panel **b** and $Ce_3Pd_{20}Si_6$ from panel **c** as shadings. **b**| A coefficient of the low-temperature electrical resistivity of $YbRh_2Si_2$ as function of applied magnetic field $B = \mu_0 H$. The inset relates the A coefficient to the Sommerfeld coefficient γ_0 and the Pauli susceptibility χ_0 and confirms the validity of the Kadowaki-Woods and Sommerfeld-Wilson ratios (adapted with permission from ref. 178). **c**| A coefficient of the low-temperature electrical resistivity of $Ce_3Pd_{20}Si_6$ vs B, evidencing mass enhancements at two distinct fields (adapted with permission from ref. 14). **d** Fermi velocity renormalization with respect to the noninteracting value from DFT vs magnetic field for the nodal-line semimetal ZrSiSe, the nodal-loop semimetal ZrSiS,

42

cont. FIG. 2: ... and graphene. **e** Correlation strength in various topological materials as quantified by the reduced Drude spectral weight compared to the DFT value. The symbol for twisted bilayer graphene (BLG) represents a prediction from the observed insulating state. References for all materials in **d** and **e** other then ZrSiSe are given in ref. 134 (adapted with permission from ref. 134).
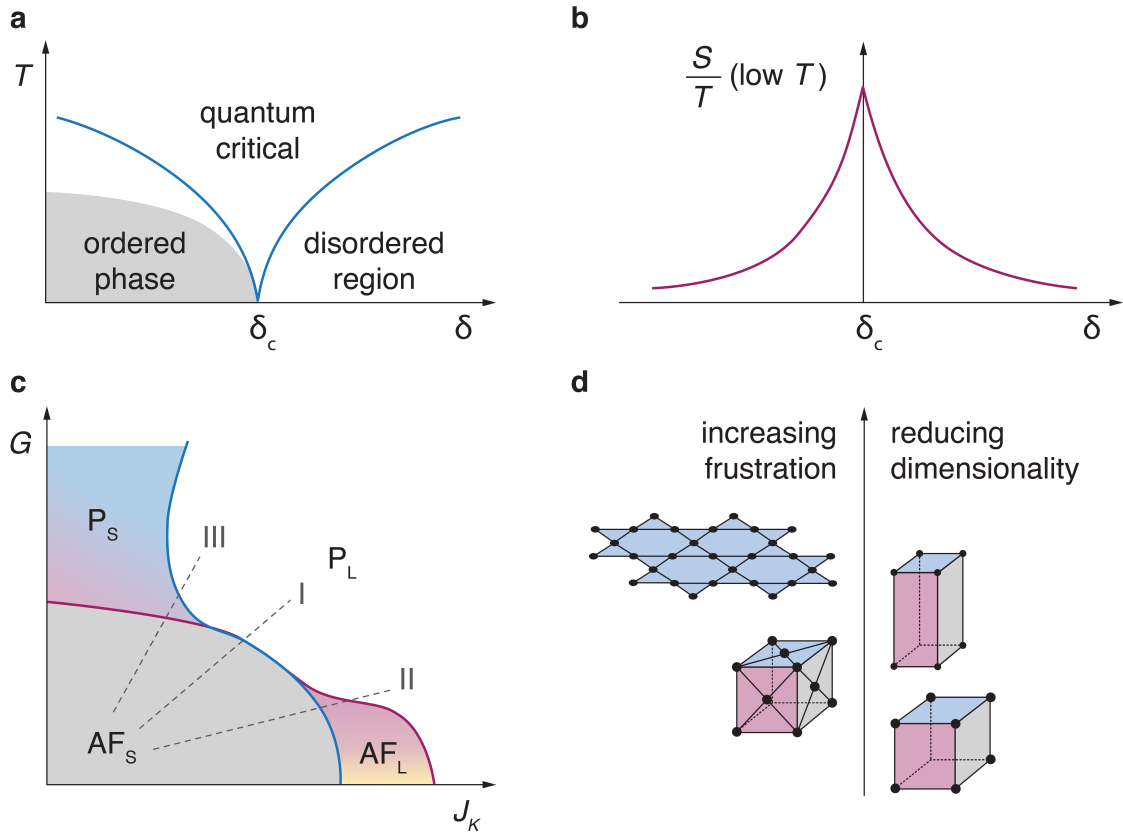
FIG. 3: **Quantum criticality. a**| Emergence of a QCP in the temperature–tuning parameter (T vs δ) phase diagram. The QCP, at zero temperature and $\delta = \delta_c$, represents the point where long-range order is continuously suppressed to zero. **b**| Evolution of the entropy S vs δ, showing that S/T at a low T is peaked near the QCP (adapted with permission from ref. 40). **c**| A global phase diagram for heavy fermion metals, where J_K tunes the Kondo coupling and G varies the degree of frustration. P and AF stand for paramagnetic and antiferromagnetic phases, while the subscripts L and S denote the Fermi surface being large and small (adapted with permission from refs. 89 and 90). **d**| Illustration of variations in the degree of geometrical frustration and in spatial dimensionality (adapted with permission from ref. 6).
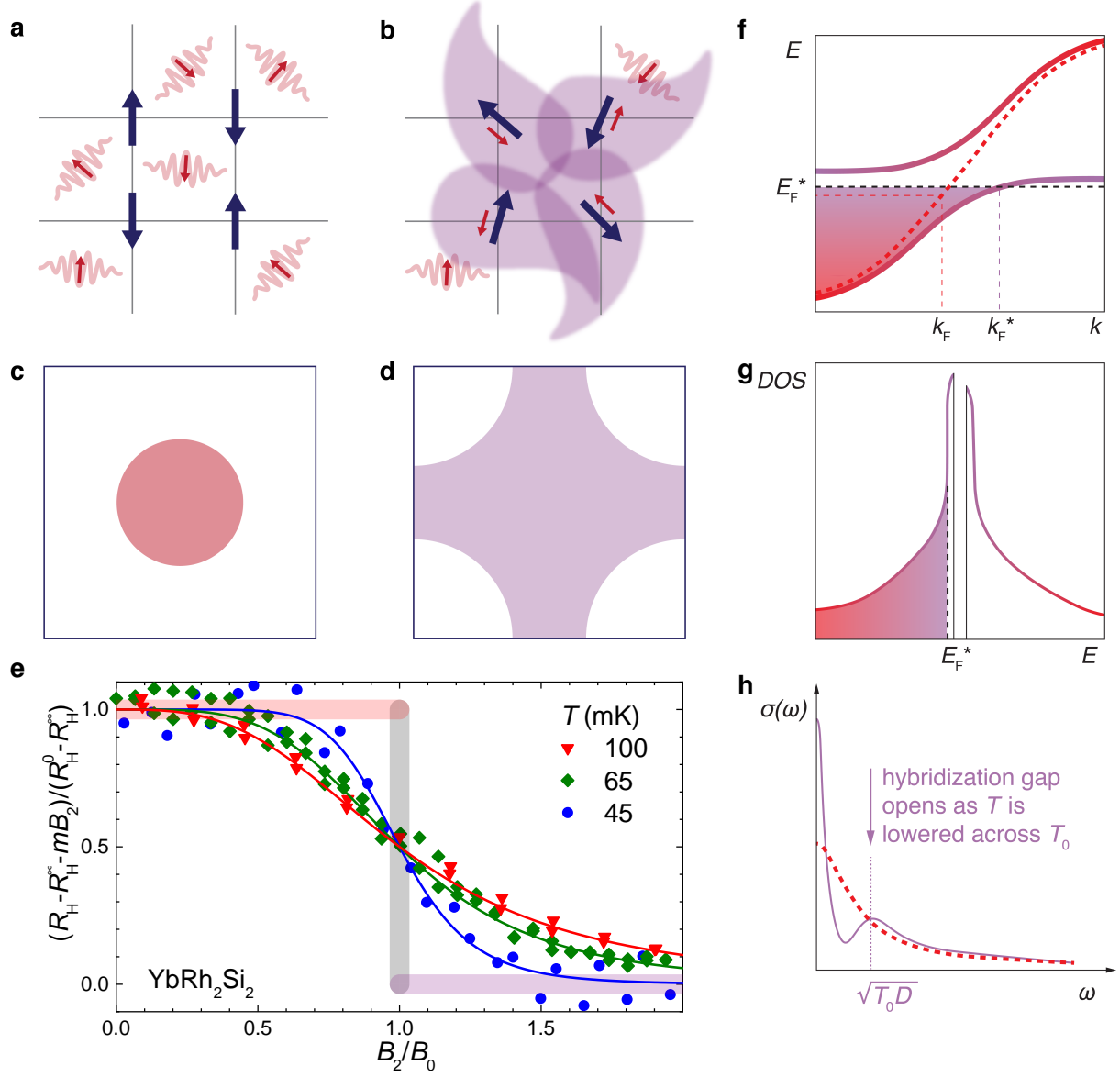
FIG. 4: **Fermi-surface jump at a Kondo destruction QCP. a-b|** Kondo lattice model, in its Kondo-destroyed and Kondo-screened phases, respectively. The dark blue arrows label the local spins, and the red arrows with wavy lines represent conduction electrons. **c-d|** Small and large Fermi surfaces, respectively. **e|** The linear-response isothermal Hall coefficient as function of a tuning magnetic field B_2. The latter is normalized by the threshold field for the QCP, B_0. The jump is the limit of extrapolating the data to the $T = 0$ limit (adapted with permission from ref. 5). **f-h|** Kondo screened state with hybridized bands, a close-up of the corresponding density of states near the gap, and its optical conductivity signature, respectively. Panel **h** is adapted with permission from ref. 34.
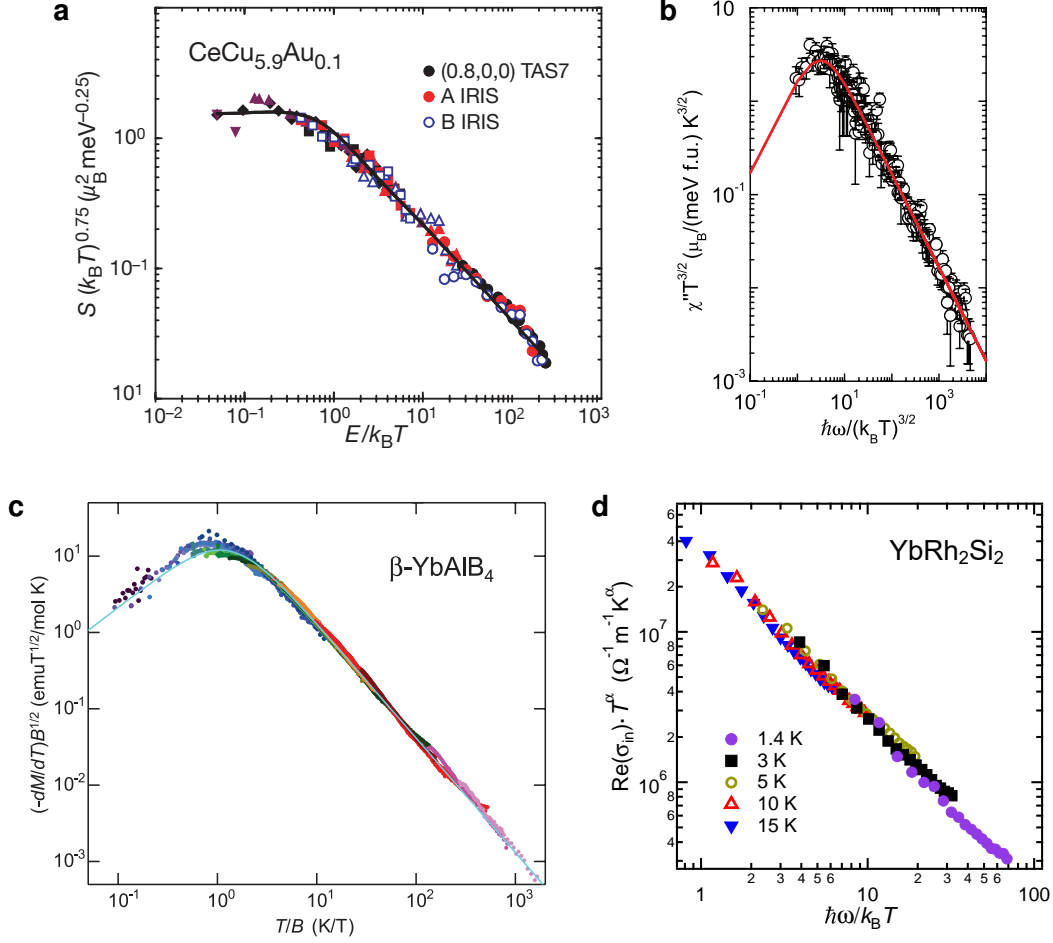
FIG. 5: **Quantum critical scaling. a-b**| Dynamical scaling in the spin dynamics of $CeCu_{5.9}Au_{0.1}$ (adapted with permission from ref. 2) and $CeCu_2Si_2$ (adapted with permission from ref. 61). **c**| T/B scaling of dM/dT, where M is the magnetization, in β-YbAlB$_4$ (adapted with permission from ref. 54). **d**| ω/T scaling in the optical conductivity of YbRh$_2$Si$_2$ (adapted with permission from ref. 7).
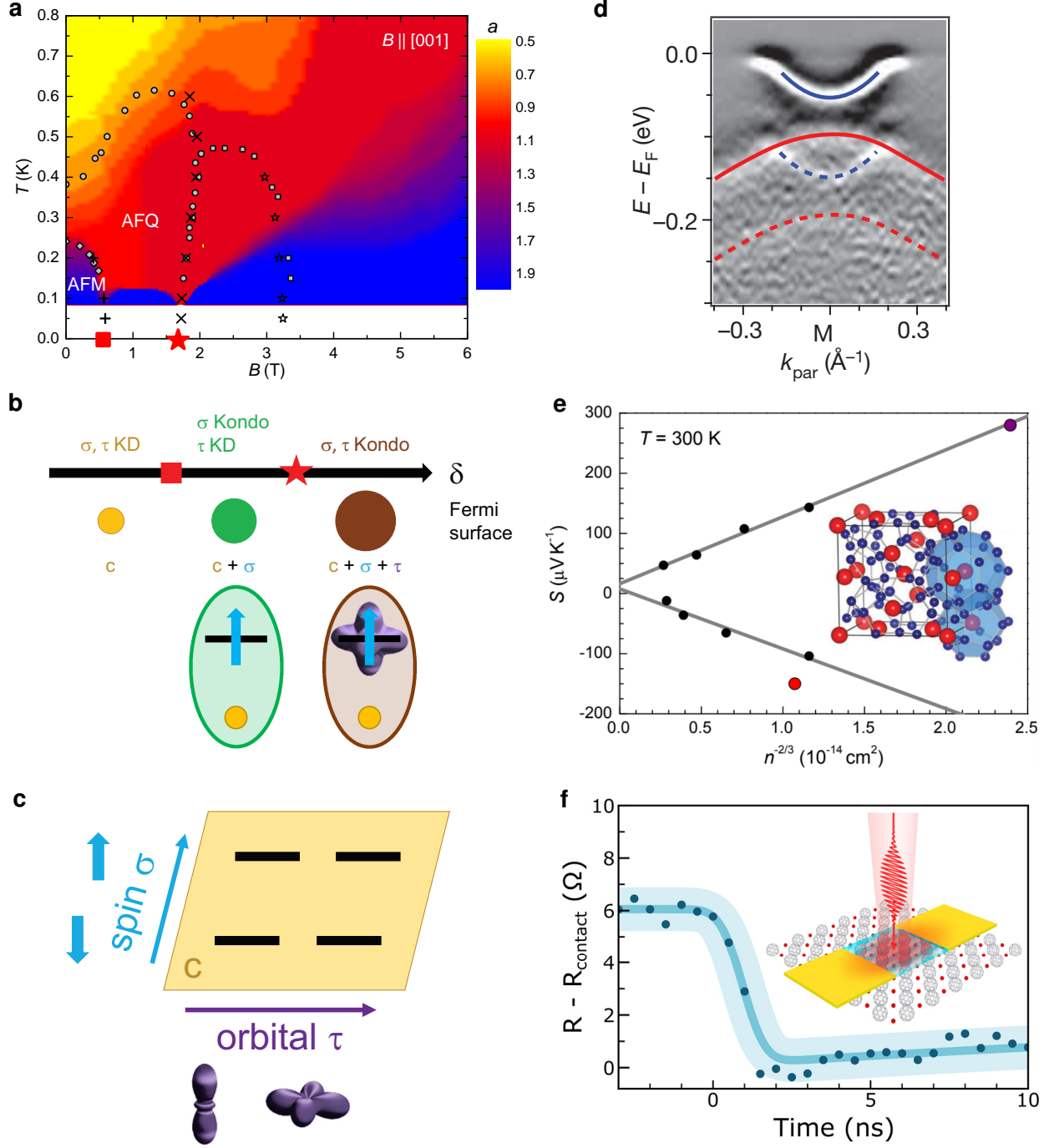
FIG. 6: **Composite and boosted interactions. a**| Temperature-tuning parameter phase diagram of the heavy fermion compound $Ce_3Pd_{20}Si_6$ (adapted with permission from ref. 14). **b**| Sketches visualizing the interaction of spin (σ) and orbital (τ) degrees of freedom with conduction electrons (c), in the form of two stages of Kondo destruction (KD, adapted with permission from ref. 14). **c**| Degrees of freedom that entangle in the Kondo phases of $Ce_3Pd_{20}Si_6$, adapted with permission from ref. 14. **d**| ARPES image of monolayer FeSe on $SrTiO_3$, revealing replica (dashed guides-to-the-eyes) of the main bands

47

cont. FIG. 6: ... (full lines, adapted with permission from ref. 168). **e|** Thermopower at 300 K of the type-I clathrate $Ce_{1.1}Ba_{6.9}Au_{5.5}Si_{40.5}$ (red symbol) compared with non-4f reference compounds (black, violet) of various charge carrier concentrations n (adapted with permission from ref. 117). **f|** Resistance of K_3C_{60} at 100 K, from a transient 2-point measurement corrected for contact contributions, vs the time after a 75 ps pump pulse (adapted with permission from ref. 174).
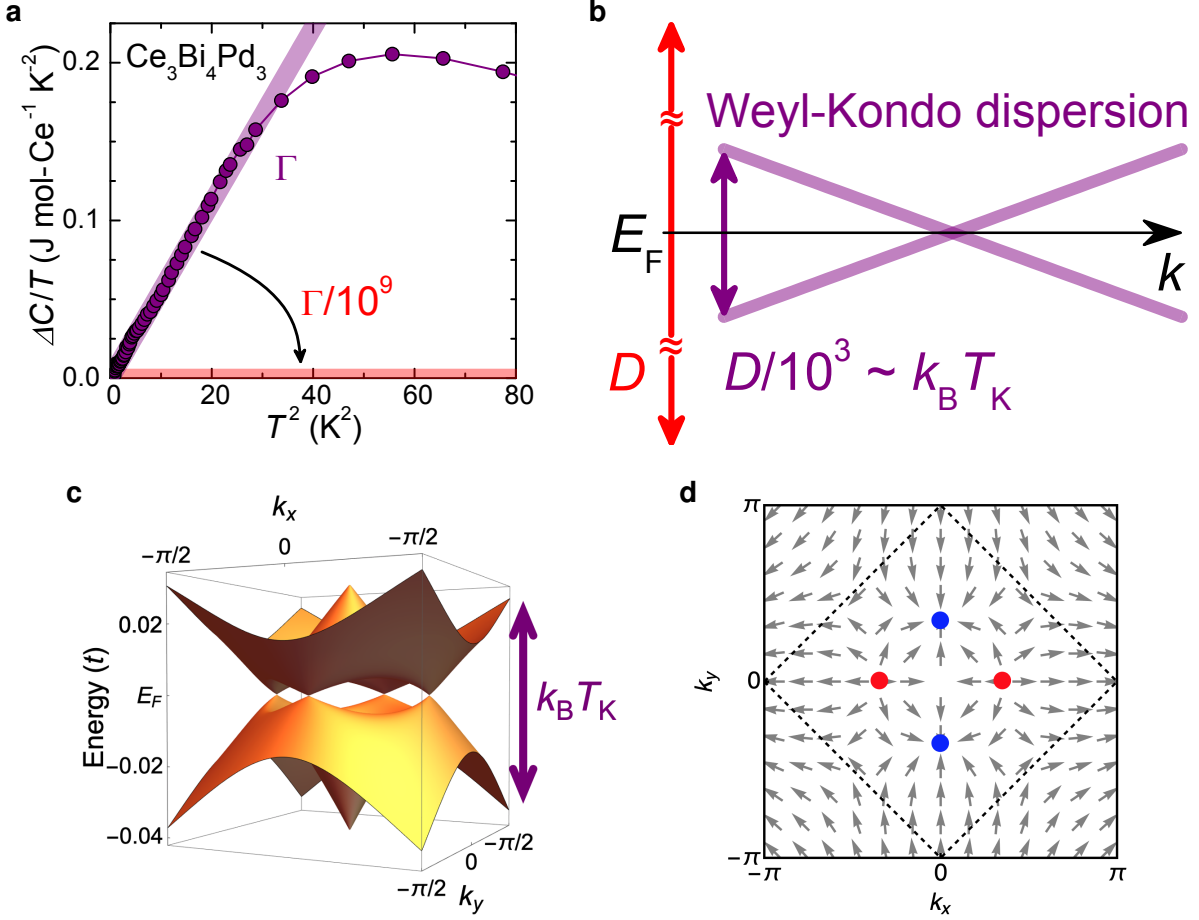
FIG. 7: **Weyl-Kondo semimetal. a**| Electronic specific heat coefficient $\Delta C/T$ of $Ce_3Bi_4Pd_3$, displaying linear-in-T^2 behavior at low temperatures (adapted with permission from ref. 18). **b**| Sketch of the linear electronic dispersion in momentum space near a Weyl point and the band renormalization corresponding to the specific heat result. **c**| Dispersion of a theoretical model for a Weyl-Kondo semimetal (adapted with permission from ref. 19).

d| Berry curvature field near the Weyl and anti-Weyl nodes (red and blue dots, respectively) for the same model (adapted with permission from ref. 19).
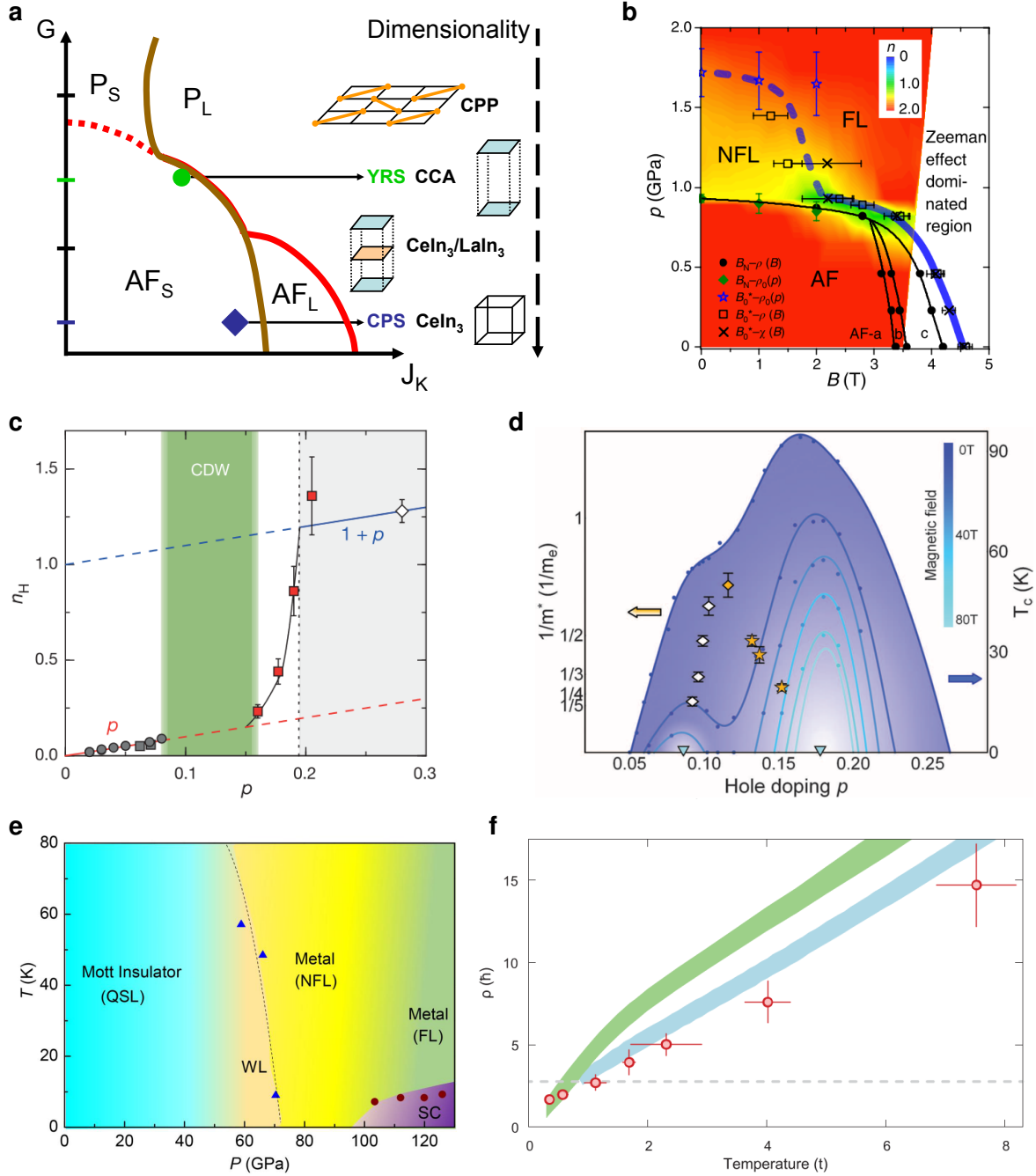
FIG. 8: **Broader implications. a**| Schematic zero-temperature phase diagram with Kondo coupling J_K and frustration parameter G axes. The phases have the same meaning as in Fig. 3c. Dimensionality (right) helps to calibrate the placement of selected materials (CPS: $Ce_3Pd_{20}Si_6$, YRS: $YbRh_2Si_2$, CCA: $CeCu_{6-x}Au_x$, CPP: Ce_2Pt_2Pb, reproduced with permission from ref. 6). **b**| Pressure–magnetic field phase diagram of CePdAl, extrapolated from finite temperature results to $T = 0$. The colour code represents n in $\Delta\rho \sim AT^n$, revealing a range of non-Fermi liquid (NFL) behavior (adapted with permission from ref. 102). **c**| Doping dependence of the Hall number in the normal state for LSCO (circles),

50

cont. FIG. 8: ... YBCO (grey and red squares), and strongly overdoped Tl-2201 (white diamond, adapted with permission from ref. 1). **d**| Inverse effective mass (yellow and white symbols, from quantum oscillations) and T_c (blue circles, from resistivity) vs hole doping in $YBa_2Cu_3O_{6+\delta}$ (reproduced with permission from ref. 112). **e**| Temperature-pressure phase diagram of $NaYbSe_2$ with regions featuring quantum spin liquid (QSL), weak localization (WL), non-Fermi liquid (NFL), superconducting (SC), and Fermi liquid (FL) behavior (reproduced with permission from ref. 155). **f**| Resistivity vs temperature of ultracold lithium-6 atoms in a two-dimensional optical lattice, from experiment (red points), finite-temperature Lanczos calculations (blue), and single-site DMFT (green); the gray line represents the upper bound on Drude resistivity (reproduced with permission from ref. 175).
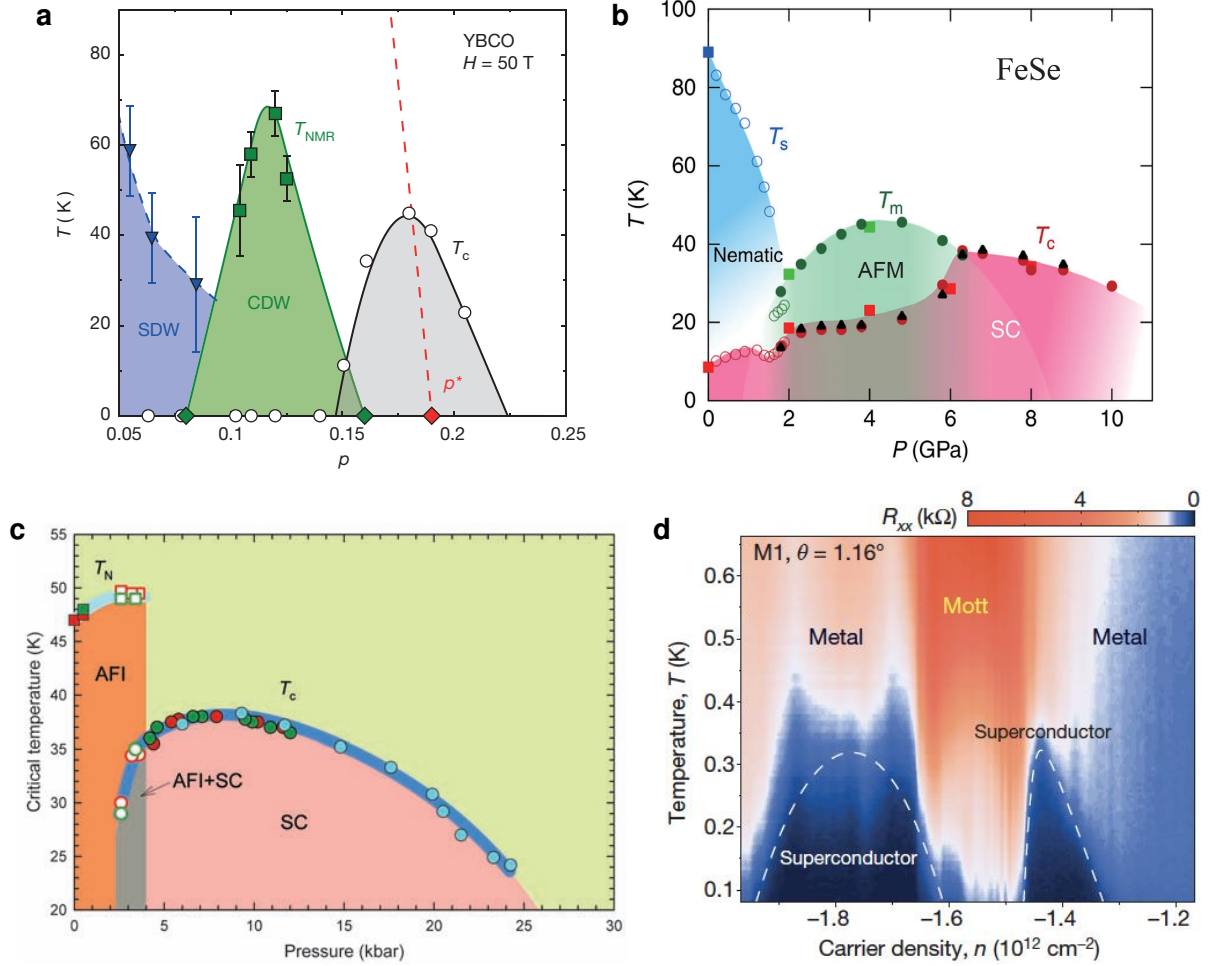
Supplementary Information

FIG. S1: **Landscape of quantum phases in strongly correlated materials. a-d|** Temperature-tuning parameter phase diagrams of the cuprate superconductor $YBaCuO_{6-\delta}$ (reproduced with permission from ref. 1), the iron pnictide FeSe (adapted with permission from ref. 179), the fulledide compound C_{60} (reproduced with permission from ref. 111), and magic angle twisted bilayer graphene (reproduced with permission from ref. 10), respectively. The different phases and functionalities result from the interplay of various low-energy degrees of freedom as illustrated in Fig. 1 of the main part.

InfoBox 1: **Heavy fermion state out of Kondo lattice**

Heavy fermion materials contain elements with partially-filled f electrons, which are coupled to spd electrons through a hybridization matrix[27]. In many cases, the count of the f electrons is fixed at an odd-integer value, because a change of their valence occupation costs too much Coulomb repulsion. For example, there would be one $4f$ electron per Ce ion or thirteen $4f$ electrons (which is equivalent to one $4f$ hole) per Yb ion. In such cases, an f electron acts as a localized magnetic moment in the low-energy description. We illustrate the physics in the simplest situation, with one spin-1/2 local moment occupying each site, each unit containing only one site, and only one spd based conduction electron band. This is the Kondo lattice Hamiltonian, which reads

$$
\begin{aligned}
\mathcal{H}_{\mathrm{KL}} &= \mathcal{H}_f + \mathcal{H}_K + \mathcal{H}_c, \\
\mathcal{H}_f &= (1/2)\sum_{ij} I_{ij}\, \mathbf{S}_i\, \mathbf{S}_j\,; \qquad \mathcal{H}_K = \sum_i J_{\mathrm{K}}\, \mathbf{S}_i \cdot \mathbf{s}_{c,i}\,; \qquad \mathcal{H}_c = \sum_{\mathbf{k}\sigma} \epsilon_{\mathbf{k}} c^{\dagger}_{\mathbf{k}\sigma} c_{\mathbf{k}\sigma}
\end{aligned}
\tag{1}
$$

At a site i, the local moment, $\mathbf{S}_i$ interacts with the spin of the conduction electron, $\mathbf{s}_{c,i} = (1/2)c^{\dagger}_i \vec{\sigma} c_i$, through an antiferromagnetic Kondo exchange coupling J_{K}. It is convenient to introduce an explicit term, I_{ij}, to describe the RKKY interaction between the local moments located at different sites. Finally, $\epsilon_{\mathbf{k}}$ describes the band dispersion of the conduction c electrons. The model can be generalized to incorporate additional complexity.

For the Hamiltonian 1, the Kondo coupling can be parameterized by a bare Kondo energy scale, $T_0 = N_{\mathrm{F}}^{-1}\exp\left(-1/J_{\mathrm{K}}N_{\mathrm{F}}\right)$ (with k_{B} being set to unity), where N_{F} is the density of states of the noninteracting conduction electron band at the Fermi energy [the corresponding Fermi momentum being marked k_{F} in (Fig. 4f)]. The RKKY interaction I_{ij} is taken to have a characteristic value I. The Doniach competition[28] is characterized by tuning the parameter $\delta = T_0/I$. Where T_0 dominates over I is the regime for the traditional description of a paramagnetic heavy Fermi liquid. In the ground state, the local moments and the spins of conduction electrons form a Kondo singlet. To describe the excitation spectrum associated with this ground state, it is convenient to rewrite the Kondo interaction at any given site to be $(1/2)\sum_{\sigma}[\sigma S^z c^{\dagger}_{\sigma} + X^{\sigma\bar{\sigma}} c^{\dagger}_{\bar{\sigma}}]c_{\sigma}$, where $\bar{\sigma} \equiv -\sigma$, and $X^{\sigma\bar{\sigma}}$ is the spin raising (lowering) operator for $\sigma = \uparrow (\downarrow)$. With a nonzero static amplitude for such a Kondo singlet, the local moment binds with the conduction electron, and $F^{\dagger}_{\sigma} = \sigma S^z c^{\dagger}_{\sigma} + X^{\sigma\bar{\sigma}} c^{\dagger}_{\bar{\sigma}}$ acts as a composite fermion. The Kondo interaction becomes a hybridization $\sum_{\sigma} F^{\dagger}_{\sigma} c_{\sigma}$. From the perspective of the conduction

electrons, $F_\sigma^\dagger$ introduces a resonance near the Fermi energy. Thus, $F_\sigma^\dagger$ is referred to as creating a Kondo resonance. In the overall electronic excitations, the composite fermion hybridizes with the conduction electron band to form the hybridized bands sketched in Fig. 4f[27]. The Fermi surface is formed by both the composite fermions and the conduction electrons, and the Fermi surface (k_F^*) becomes large. The composite fermions lead to a density of states with a sharp peak near the Fermi energy (see Fig. 4g), which spreads over a narrow energy range determined by the Kondo scale.

The scale T_0 is also reflected in the evolution of the excitation spectrum as a function of temperature. At temperatures much larger than T_0, the local moments and conduction electrons are essentially decoupled. As temperature is lowered through T_0, the Kondo correlation between the two species of spins start to set in. This leads to the initial onset of a "hybridization gap", as would be seen in the optical conductivity $\sigma(\omega)$ (see Fig. 4h). The corresponding frequency scale is $\sqrt{T_0 D}$ (where D is the conduction electron bandwidth) is determined by the zero-wavevector (direct) transfer transition between the occupied and empty states in the hybridized bands.

InfoBox 2: **Noninteracting electronic topology.**

Weyl semimetals are materials in which bulk energy bands touch only at discrete points in momentum space (the Weyl nodes) and where, in the vicinity of the nodes, the electron wave functions of these two bands can be approximated by the Weyl equation, which has far-reaching consequences. In the pertinent lattice theory of chirally invariant fermions with locality, there is an equal number of production and annihilation of Weyl fermions[180]. Thus, Weyl nodes with Weyl fermions of opposite chirality occur in pairs such that the axial charge is conserved. The nontrivial topological nature of a Weyl semimetal guarantees that the two nodes of such a pair are separated in momentum space. Experimental observables include the linear bulk dispersion near the Weyl nodes, surface Fermi arcs that connect the projection of two bulk Weyl nodes of different chirality in the surface Brillouin zone, the chiral anomaly manifesting in an extremely large negative longitudinal magnetoresistance, or the monopoles and an antimonopoles of Berry flux in momentum space leading to spontaneous or anomalous Hall responses. Space group symmetry plays an important role in the emergence of Weyl nodes in a robust way[125,181,182]. ARPES is playing a key role in the identification of weakly-interacting topological electronic materials. As a highly surface sensitive technique it is particularly well suited to probe topological surface states. Indeed, an APRES investigation of the (111) surface of the topological insulator Bi_2Se_3 revealed, with amazing clarity, a single Dirac cone in the surface electronic band dispersion (**a**, adapted with permission from ref. 183). If higher energy photons are used, ARPES acquires some bulk sensitivity. It has thus also been used to probe topological bulk bands. Examples are the identification of a bulk Dirac cone in Na_3Bi (**b**, adapted with permission from ref. 184) and of two closely spaced Weyl cones in TaAs (**c**, adapted with permission from ref. 185). In the latter, crescent-shaped surface states (**d**, adapted with permission from ref. 185) were assigned as being the topological Fermi arcs that connect the surfaces projections of the bulk Weyl nodes (+ and − in panel **c**). That there are two arcs is attributed to two pairs of bulk nodes collapsing in the surface projection.